Journal of Petroleum Science and Engineering 197 (2021) 108103

Contents lists available at ScienceDirect

Journal of Petroleum Science and Engineering

journal homepage: http://www.elsevier.com/locate/petrol

Restoration of annular zonal isolation using localized casing expansion (LCE) technology: A proof of concept based on laboratory studies and field trial results

T.K.T. Wolterbeek [a], E.K. Cornelissen [b], S. Nolan [c], F. Todea [c], W. Stam [b], S.M. Roggeband [b], L. Dam [b], E.J. van Riet [b], F. Ruckert [b], W.J.G. Keultjes [b,*]

[a] HPT Laboratory, Department of Earth Sciences, Utrecht University, Princetonlaan 4, CB Utrecht, 3584, the Netherlands
[b] Wells Technology, Shell Global Solutions International B.V., Grasweg 31, HW Amsterdam, 1031, the Netherlands
[c] Shell Canada Limited, Calgary, Canada

ARTICLE INFO

Keywords:
Well integrity
Well abandonment
Sustained casing pressure
Surface casing vent flow
Annular fluid migration
Casing expansion

ABSTRACT

Sustained casing pressure (SCP), surface casing vent flow (SCVF) and other expressions of annular fluid migration are widely encountered zonal isolation issues. Conventional solutions for SCP/SCVF include perforate and squeeze cementing, or section milling and recementing. Regrettably, the former approach shows only limited success rates, while the latter involves time and cost intensive operations that require a drilling rig. We will show that localized casing expansion (LCE) technologies offer promising alternatives, enabling rigless remediation of annular fluid migration. The LCE concept involves imposing permanent deformation on the casing pipe to locally enlarge its diameter. The associated annular volume reduction causes closure of defects such as micro-annuli and cement fractures, plus potentially even larger voids, and results in an overall densification of the cement microstructure. The Shell-developed Local Expander tool is e-line deployable and imposes the required casing deformation in a mechanical, fully controlled manner. Tailored-shaped energetic charges offer valuable supplementary means for achieving expansion. We will demonstrate the sealing effectiveness of LCE in both laboratory experiments and field trials, describe how the radial deformation impacts the casing and cement, and generally discuss the current state of knowledge, capabilities and limitations of LCE with respect to SCP/SCVF remediation.

1. Introduction

With many oil and gas reservoirs nearing the end of their economic and productive lifetime (Kaiser, 2015; Liversidge et al., 2006; Warne, 2004), there is a growing need for effective wellbore plugging and abandonment (P&A) procedures (Barclay et al., 2001; Campbell and Smith, 2013; Vrålstad et al., 2019). Achieving robust zonal isolation, i.e. ensuring unwanted fluid migration along the well trajectory is prevented long-term, is a key P&A objective. Zonal isolation must be achieved to prevent seepage into the environment or potable water resources (Smith et al., 2011) and maintain reservoir containment for future reuse, e.g. in CO_2 sequestration (Wolterbeek et al., 2019; Wolterbeek and Raoof, 2018; Zhang and Bachu, 2011) or energy storage applications (Bauer et al., 2013; Hou et al., 2013; Procesi et al., 2013).

In typical well designs, the borehole is lined with nested strings of steel casings and liners, which are fixed in place and sealed against each other and the rock formations using low-permeability Portland cement. These cement sheaths, while engineered to provide adequate zonal isolation, are susceptible to several types of failure (Gasda et al., 2004). Structural flaws such as fractures in the bulk cement or debonding at casing-cement and cement-rock interfaces undermine sealing and can result from various causes, starting with substandard well construction or P&A operations (Barclay et al., 2001; Dusseault et al., 2000). Incomplete removal of drilling mud or filter-cake before cement placement, for example, may impair sealing integrity due to mud channel (macro-annulus) formation or reduced cement-formation bond quality (Agbasimalo and Radonjic, 2014; Ladva et al., 2005). Shrinkage inherent to the hydration and setting of conventional (non-expanding) Portland cements (Bosma et al., 2000; Chenevert and Shrestha, 1991; Jandhyala et al., 2018; Reddy et al., 2007; van Eijden et al., 2017)

* Corresponding author.
E-mail address: wout.keultjes@shell.com (W.J.G. Keultjes).

https://doi.org/10.1016/j.petrol.2020.108103
Received 23 September 2020; Received in revised form 28 October 2020; Accepted 1 November 2020
Available online 9 November 2020

produces a bulk volumetric contraction that can create debonding microannuli along casing-cement and cement-formation interfaces (Dusseault et al., 2000; Torsæter et al., 2015; van Eijden et al., 2017). Even if high-quality cement is placed without deficiencies and initially provides a good seal, changes in the temperature or mechanical loading subsequently experienced by the wellbore due to production or stimulation may lead to progressive accumulation of damage (Kuanhai et al., 2020; Lecampion et al., 2013; Orlic, 2009; Ravi et al., 2002; Wise et al., 2020; Wolterbeek et al., 2016; Zeng et al., 2019). Internal casing pressure cycling, for example, is known to cause debonding microannuli along interfaces and radial cracks in the cement sheath (Boukhelifa et al., 2005; Goodwin and Crook, 1992; Heathman and Beck, 2006).

The extent to which sealing integrity is impacted by the aforementioned processes depends on various factors, including the properties of the hydrated cement, the geometry of the casing string, and the behaviour of surrounding rock formations (Arjomand et al., 2018; Bois et al, 2010, 2018; Bosma et al., 1999; Griffith et al., 2004; Wang and Taleghani, 2014). Regardless of how damage is incurred, if sufficiently interconnected, structural flaws in and around the cement may offer pathways for annular fluid migration. Such unwanted seepage can manifest itself at the wellhead as surface casing vent flow (SCVF), sustained casing pressure (SCP) or gas migration (GM) (Nelson and Guillot, 2006). These phenomena are widely encountered zonal isolation issues, though the statistics of their occurrence vary significantly between available datasets and depend on exploitation history, regulatory history, basin geology and wellbore age, design and status (Davies et al., 2014). Among nearly 440,000 wells that have been drilled in Alberta, Canada since 1910 about 5% record SCVF/GM (Bachu and Watson, 2006; Natural Resources Canada, 2019). Note this includes about 7% of abandoned wells (Boyer, 2016 in Natural Resources Canada, 2019). Analysis of compliance reports for 41,381 wells drilled in Pennsylvania, USA between 2000 and 2012 showed that ~1.9% of these wells exhibited some form of integrity failure (Ingraffea et al., 2014). Based on United States Minerals Management Service data, about 43% of ~15,500 wells located on the outer continental shelf of the Gulf of Mexico (period 1973–2003) reported SCP on at least one casing annulus (Brufatto et al., 2003). Remedial measures are required if SCP exceeds the maximum wellhead pressure allowed by regulations or exceeds well design criteria (Bourgoyne et al., 1999) or, equivalently, if SCVF exceeds acceptable flow rate or fluid composition limits. In any case, known impairments of zonal isolation must be remediated prior to abandonment (Barclay et al., 2001).

Conventional approaches to SCP/SCVF remediation include perforate and squeeze cementing operations (Slater, 2010; Toor, 1983) and cutting-pulling or section milling of the casing plus recementing (Joppe et al., 2017; Nelson et al., 2018; Obodozie et al., 2016). Squeeze cementing involves forcing cement slurry, under pressure, through perforations in the casing into the target annular space or rock formation, in order to seal off fractures, voids and other defects (Fuller et al., 2016; Nelson and Guillot, 2006). Unfortunately, this method is often ineffective. A performance study analysing the effectiveness of squeeze cementing operations conducted on wells in West Texas, USA found a first-attempt success rate of only 34% (47 of 137 cases), while the overall success rate for multiple attempts, up to five per well, did not exceed 60% (Cowan, 2007). Studies on squeeze cementing operations in Alberta, Canada and the Gulf of Mexico report success rates of around 50% (Saponja, 1999; Wojtanowicz et al., 2001). Surfactant treatment may improve squeeze cementing efficacy, but multiple attempts typically remain needed (Winarga and Dewanto, 2010). In some jurisdictions, section milling and under-reaming is preferred and often required when annular fluid migration cannot be adequately remediated via other means (Nelson et al., 2018). This method allows the casing and cement to be removed over a specified interval, enabling subsequent placement of a rock-to-rock cement plug. While this may be a relatively reliable approach (Obodozie et al., 2016), removal of the casing by milling or pulling requires a drilling rig and is generally a complex (e.g. swarf handling) and time-consuming, thus costly operation.

Given the above, there is clear scope for alternative approaches that allow reliable remediation of annular fluid migration. One possible method is to impose deformation on the innermost casing pipe and permanently enlarge its diameter, as the associated reduction in annular volume would bring about compressive closure of micro-annuli and fractures, plus potentially even larger defects, while producing an overall densification of the cement microstructure. This so-called casing expansion concept was first explored by Kupresan et al. (2014, 2013), who performed three lab experiments on ~60 cm long composite samples consisting of two concentric steel tubes with annular cement (outer pipe: 101.6 mm outer diameter, 5.7 mm wall thickness; inner pipe: 60.3 mm outer diameter, 2.8 mm wall thickness). Initial annular sealing in these samples was poor due to the presence of micro-annuli along the casing-cement interfaces, resulting in equivalent permeabilities of 1.4×10^{-13} to 7.0×10^{-12} m^2. The inner pipe was subsequently lubricated and radially enlarged by 2–8%, over the entire length of the sample, using a conical expansion mandrel. This led to noteworthy reductions in equivalent permeability, which attained 3×10^{-19} m^2 in the initially most permeable sample and reached values below detection in the others (Kupresan et al., 2014). Post-experiment analysis showed that deformation in the cement sheath was accommodated by a combination of pore collapse, structural reconfiguration of the cement matrix, and displacement of free pore fluid. Note small perforations made in the outer pipe of the samples allowed for cement extrusion and relief of excess fluid pressure during the expansion process (see Fig. 8 of Kupresan et al., 2014).

While the work of Kupresan et al. (2014, 2013) established the sealing potential of casing expansion, the swaging method they used to achieve the required pipe enlargement in their experiments is not easily deployed in practice, particularly in existing wellbores (Wolterbeek et al., 2018). Commonly-used casings and especially conventional casing connections are simply not designed and too bulky for expansion using a pull-through or hydraulically driven expansion cone (DeLange et al., 2011). Even for solid expandable tubular technology (Bailey, 2009; Filippov et al., 1999), which could possibly be installed as part of remedial measures (Bargawi et al., 2005), expanding successfully against fully set cement would be far from trivial if not unfeasible (Fanguy et al., 2004). The swaging process will be complicated further by mineral scaling and other lubrication issues (Di Crescenzo et al., 2015), as frictional forces may cause cone expansion to induce damage in the casing pipe (Byrom, 2014). Localized casing expansion (LCE) technologies (cf. Cornelissen, 2019; Duncan, 2019; Kunz, 2017) overcome these difficulties by imposing the radial enlargement over longitudinally limited lengths of casing, e.g. as local indentations or “dents”, bulging out the casing into the surrounding cement. Placement of multiple such dents allows intervals of cement sheath to be axially constrained, enabling effective cement compression and closure of micro-annuli and fractures in the cement over longer length scales. The Shell-developed Local Expander tool imposes the required indentations in a mechanical, fully controlled manner (Cornelissen, 2019). A technology being developed in parallel, called the Energetic Expander tool, makes use of tailored shaped explosive charges to achieve similar localized expansions (Ruckert, 2020). In this paper, we will describe these two LCE technologies, demonstrate their sealing effectiveness in both laboratory experiments and field trials, discuss how the imposed radial deformation impacts casing and cement, and generally assess the current state of knowledge, capabilities and limitations of LCE with respect to SCP/SCVF remediation.

2. Local Expander tool description

The Local Expander tool is an e-line deployable technology that can impose very localized, approximately ring-shaped radial deformations on casing pipe (Cornelissen, 2019). A schematic diagram of a 7″-model of the Local Expander tool is shown in Fig. 1. The head of the tool

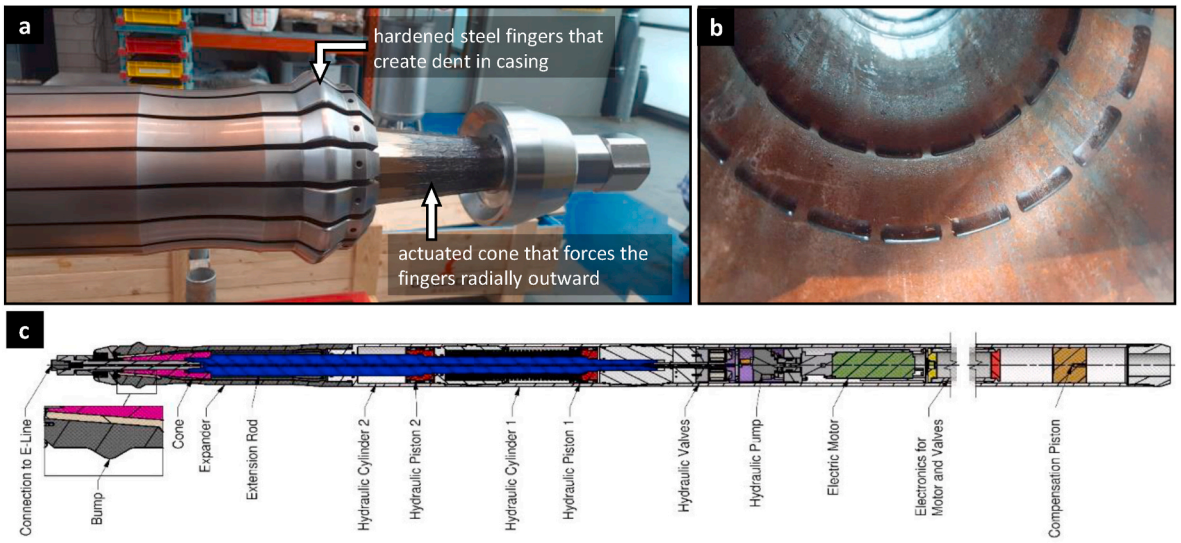

Fig. 1. Overview of a 7″-model Local Expander tool, with a) photograph of an expander element with sixteen hardened steel fingers and actuated cone, b) photograph of the indentation marks visible on the inside of a casing pipe after Local Expander deployment (note the marks line up into rings), c) schematic cross-section of the complete Local Expander tool, showing the expander head, hydraulic pistons and balancing cylinder.

consists of an expander element with sixteen hardened steel fingers (Fig. 1a), which in their collapsed, unexpanded configuration allow the tool to be freely moved up and down through the wellbore. Once in position at a selected depth, the fingers of the expander element are pressed radially outward by an actuated cone (Fig. 1a) driven by a series of double-acting hydraulic cylinders located in the main body of the tool (Fig. 1c). As the fingers move out, the casing pipe is locally deformed plastically, creating a dent (Fig. 1b and Fig. 4). The fingers are subsequently retracted by reversing flow in the hydraulic cylinders. It takes about 15 min to complete the indentation process, independent of the axial force imposed in order to create the dent. Progression can be monitored real time by tracking the electric current drawn by the tool. The shape of the resulting dent and its impact on the surrounding cement will depend on the grade, size and weight of the casing pipe. Generally, however, the longitudinal extent over which the outer surface of the casing is deflected by a single indentation will be in the order of 10 cm. It should be noted that the cement is affected over considerably longer lengths, though, particularly once the cement sheath is axially confined due to placement of multiple dents. Dents are therefore preferably placed in sets of three, with the middle dent placed last, in order to maximise defect closure and cement densification over the length of cement located in between the first two dents. The Local Expander tool is pressure compensated, so that tool performance does not vary with application depth. Various Local Expander tool models and expander element head types are available or currently being developed for use in different casing size ranges (Table 1, Appendix A).

3. Energetic expander tool description

Energetic Expander technology can impose localized casing deformations similar to the Local Expander tool. The Energetic Expander tool is deployable using e-line or digital slick line on a standard tool string equipped with a casing collar locator, weight bar, two centralizers and a shock sub. Developed in collaboration with W.T. Bell International, Inc., the Energetic Expander tool design (Fig. 2) is based on a modified shaped-charge explosive pipe cutter (Rairigh, 2020a, 2020b). Instead of cutting a tubular, the shaped charge configuration is tailored to create a pressure wave that causes plastic deformation and localized enlargement of the casing pipe without inducing material failure (Ruckert, 2020). This method of expansion also enables application in wellbore geometries that preclude use of the Local Expander tool, e.g. due to inner diameter (ID) restrictions or small running clearances. Two versions of the Energetic Expander tool exist, namely single-shot (EE-SS) and multi-shot (EE-MS) tools. The latter is equipped with three explosive charges, spaced 30 cm apart, allowing for simultaneous placement of a complete set of dents in a single tool run. The fixed dent spacing of the EE-MS tool also alleviates the requirement of high-accuracy depth control for the placement of multiple dents in close proximity, enabling deployment on slick-line. The Energetic Expander tool is currently available for casing pipe ranging from 3 to 1/2″ to 7” nominal size (= 8.9–17.8 cm OD).

Table 1
Overview of Local Expander tool specifications. OD denotes outer diameter; * ‘OD head (collapsed)’ corresponds to the minimum required casing inner diameter (ID) drift size, required for the tool to move freely up and down the bore. The “C” and “T” in expander head type names denote newer, improved designs.

Local Expander tool	4-1/2″-model				7″-model					9-5/8″-model		
expander head type (= target casing OD)	4-1/2″	4-1/2″T	5-1/2″	5-1/2″CT	7″	7″CT	7-5/8″CT	9-5/8″	9-5/8″CT	9-5/8″CT	10-3/4″CT	13-3/8″CT
OD body [mm]	90	90	90	90	143	143	143	143	143	207	207	207
OD head (collapsed)*[mm]	92.0	90.0	109.0	108.0	153.0	153.0	168.0	212.7	210	210.0	231.0	304.8
OD head (expanded) [mm]	114.6	117.1	139.5	144.9	177.4	187.0	202.0	237.1	244	306.0	327.0	400.8
max. radial increase [mm]	11.3	13.6	15.2	18.5	12.2	17.0	17.0	12.2	17	48.0	48.0	48
max. stroke length [mm]	177	177	177	177	140	140	140	140	140	425	425	425
max. axial force [kN]	853	853	1192	1192	1438	1438	1438	1438	1438	3155	3155	3155
tool length [m]	7	7	8.5	8.5	4	4	4	4	4	4.7	4.7	4.7
tool weight [kg]	~300	~300	~350	~350	~350	~350	~350	~350	~350	~750	~750	~750

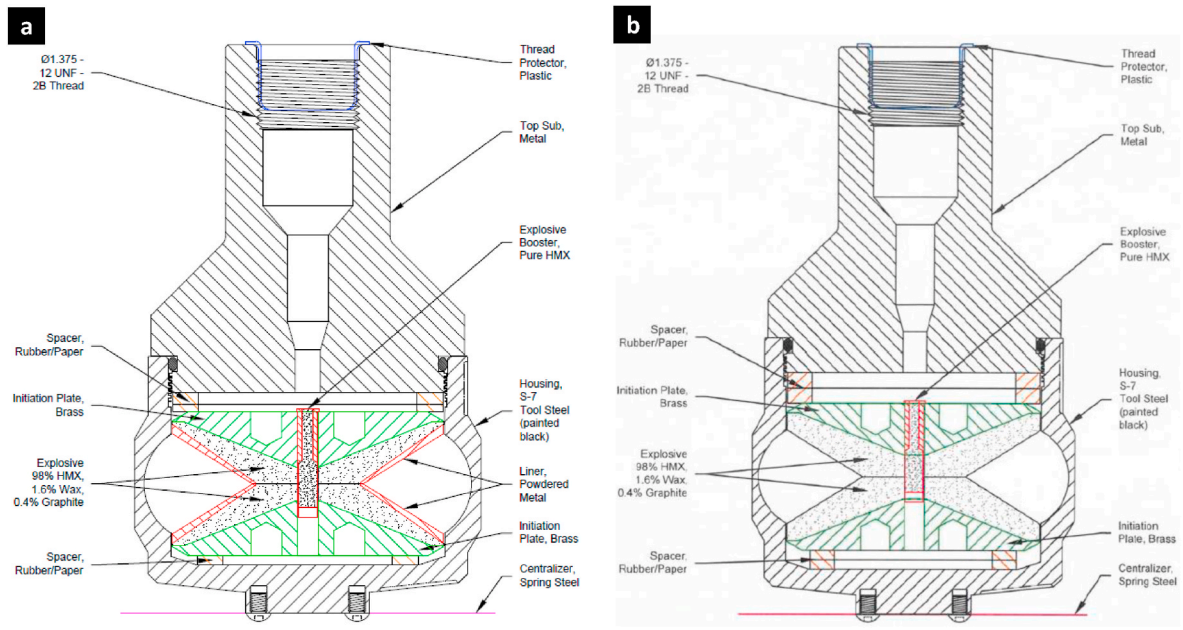

Fig. 2. Schematic cross-sections through a) conventional shaped charge pipe cutter design (with liners) and b) the new Energetic Expander tool (no liners), designed to locally enlarge the casing pipe diameter without inducing casing fracture (Figure courtesy of W.T. Bell International, Inc.).

4. Laboratory and modelling programme

4.1. Sealing performance experiments

To assess the SCP/SCVF-remediation capabilities of the Local Expander and Energetic Expander tools, a range of sealing performance experiments has been conducted. These laboratory tests involved full-scale composite samples, constructed from nested casing sections with annular cement, closely simulating intervals of cemented wellbore. All samples were created using conventional Class G Portland cements, prepared in accordance with API RP 10B-2 (ISO 10426-2, 2005), using a water-to-cement mass ratio of 0.44. The used samples were made to contain micro-annuli along casing-cement interfaces, to ensure their initial condition was permeable, i.e. represented situations of impaired zonal isolation. Laboratory testing generally involved the following steps. After establishing the initial transport properties of the wellbore sample in a flow-through experiment, the LCE technologies were deployed to locally enlarge the diameter of the inner casing. Following placement of one or more (sets of) dents, their impact on sealing performance along the sample was assessed in a second flow-through experiment. After test completion, several samples were sectioned or cored for visual inspection and microstructural study. Below we will present more detailed accounts for two examples of the sealing performance tests conducted.

4.1.1. Dual annulus laboratory testing of the Local Expander tool

The sealing effectiveness of the Local Expander tool has been investigated in a dual annulus configuration. The 1.48 m-long wellbore sample used for this test was made by concentrically nesting a K55 casing section (7″ OD, 23 lb/ft = 17.78 cm OD, 34.23 kg/m) inside two L80 casing sections (9-5/8″ OD, 53.5 lb/ft = 24.45 cm OD, 79.61 kg/m, and 13-3/8” OD, 68 lb/ft = 33.97 cm OD, 101.20 kg/m), mounted on a steel bottom flange. After cement placement, two ring-shaped steel flanges equipped with pressure line connections were welded on top of the casing sections, allowing independent pressure control in the two annuli. The cement was allowed to cure at ambient temperature under 20 bar static water pressure for 24 h. After slow depressurization, the sample was allowed to cure further for about two months. Shortly prior to testing, the disc-shaped bottom flange was removed to expose the downstream end of the sample to atmospheric pressure (Fig. 3). Reference flow-through measurements were made in order to establish the initial transport properties of each of the annuli, separately, measuring the flow rate resulting from application of N_2 pressure at the top end of the sample.

After characterization of the original sample state, a 7″-model Local Expander tool with standard head type (Table 1) was used to create a set of three dents, placed sequentially at locations about 34 cm, 94 cm and 64 cm away from the upstream end of the sample. As explained, this sequence was designed to axially lock the cement in place with the first two dents, with the intention to maximise cement densification upon placement of the third dent in between. How this procedure affected the transport properties of the annuli was subsequently evaluated in a second series of flow-through measurements. The Local Expander tool was later used to impose a fourth dent, located about 50 cm from the inlet, i.e. in between dents one and three, after which a third permeametry test was conducted.

4.1.2. Laboratory testing of the energetic expander tool

The Energetic Expander tool was tested using a 1.3 m-long sample consisting of two concentrically nested L80 casings (4-1/2″ OD, 12.6 lb/ft = 11.43 cm OD, 18.75 kg/m, and 7” OD, 26 lb/ft = 17.78 cm OD, 38.69 kg/m) with annular cement. Cementing and flow-through testing of the annulus were performed in the large-scale zonal isolation test facilities previously described by Van Eijden et al. (2017). The cement was cured at 80 °C and 100 bar N_2 pressure, for three days, using an inflatable mini-packer as a base. Following curing, this mini-packer was deflated to create access to the entire annulus below the cemented interval, enabling flow-through testing. The initial transport properties of the sample were determined by measuring the flow required to maintain the N_2 pressure at the bottom of the sample, while imposing a pressure difference across the sample (ΔP) by decreasing the N_2 pressure at the top.

After establishing its initial properties, the sample was slowly cooled down and depressurised, and subsequently removed from the zonal isolation test setup, for deployment of the Energetic Expander tool. In a separate vessel, a 68.4 mm OD tool equipped with explosive charges was used to create a single dent, located at roughly halfway the length of the cemented section. The energetic expansion process was performed at

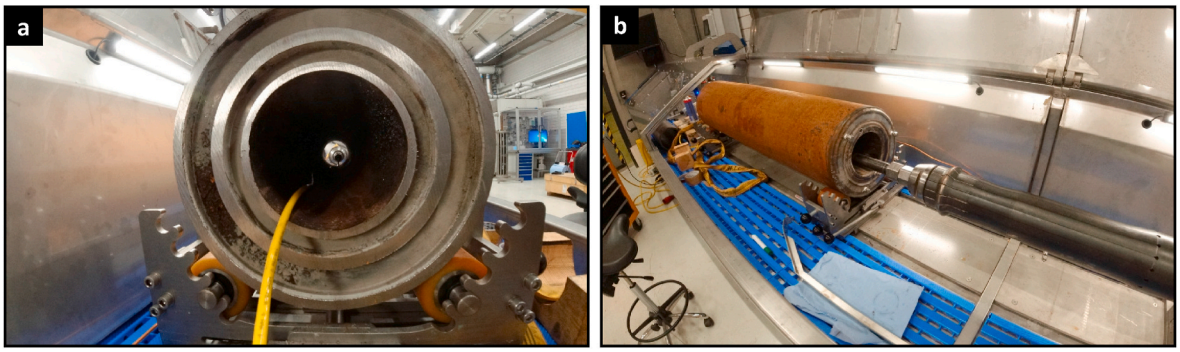

Fig. 3. Photographs of the dual annulus laboratory test of the Local Expander tool, with a) end-view of the sample, showing the three casing pipes and the cemented annuli, b) photograph of the sample (left) and the Local Expander tool head (right).

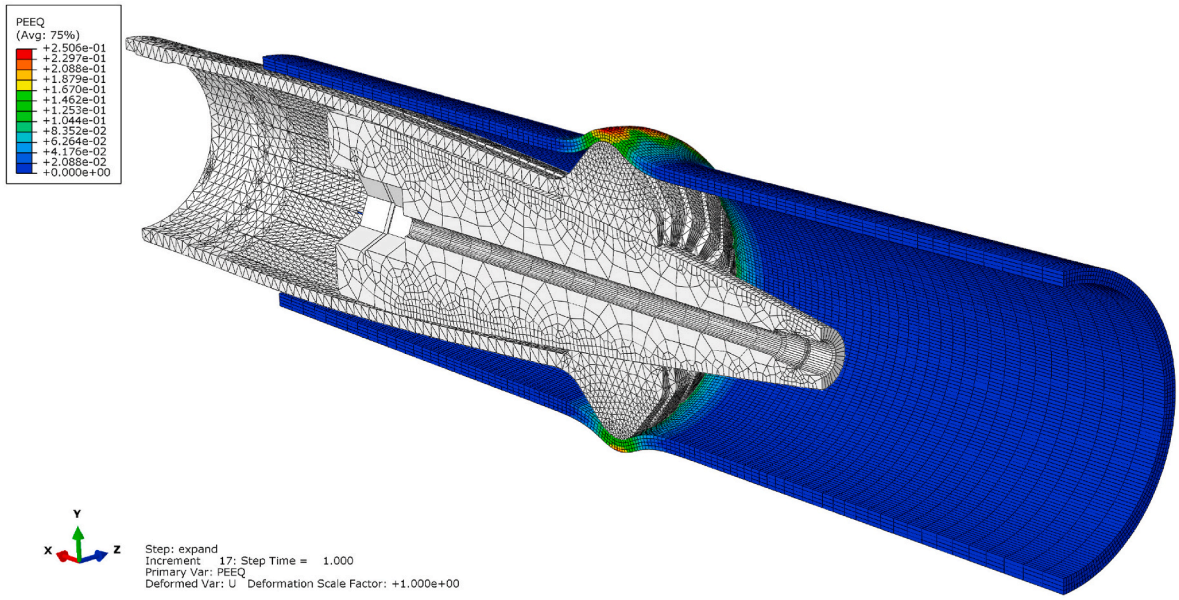

Fig. 4. Finite element model of the Local Expander tool head and a casing pipe. Note the modelled pipe has initial ovality and wall thickness imperfections that are symmetric about the x-y plane.

ambient temperature and under 100 bar water pressure. Afterwards, the sample was reinstalled in the zonal isolation setup and subjected to a second test, in order to evaluate whether annular sealing improved. This experiment was performed at 80 °C and 50 bar background N_2 pressure, again measuring gas flow as a function of pressure difference imposed.

4.1.3. Post-experiment cement characterization

While we consider the sealing performance test results leading in evaluating whether LCE-technologies can repair the hydraulic barrier function of cemented annuli, an additional aim of the laboratory testing was to assess the impact of LCE-induced deformation on the physical integrity of the cement sheath. To this end, various cement samples and subsections of casing-cement interface obtained from the sealing performance studies and other tool functionality tests have been subjected to visual inspection and microstructural analysis. Conducted analyses include optical (reflected light) microscopy and X-ray computed tomography (XRCT).

4.2. Casing integrity studies

LCE technologies impose large stresses and strains on the casing pipe to locally enlarge its diameter. The associated deformations could affect the strength of the casing. Aside from evaluating the primary functionality of LCE technologies in sealing performance tests, specific studies were performed in order to assess the impact of LCE-induced deformations on casing integrity.

4.2.1. Modelling of indentation process and subsequent burst or collapse failure

How the presence of LCE-induced dents impacts the burst and collapse strength of a casing has been investigated by means of finite element analysis (FEA), performed using ABAQUS commercial software. The FEA modelling involved simulation of the entire LCE process, including radial extension and retraction of the Local Expander tool, followed by simulation of burst or collapse loading. Various L80 casings (9-5/8" OD = 24.45 mm OD) have been simulated, where the pipe weight was varied between 36.0 and 61.1 lb/ft (= 53.57–90.93 kg/m). These nominal casing dimensions were augmented by representative pipe shape imperfections (0.5% ovality, 10% wall thickness variation as result of eccentricity), uniformly applied along the pipe length. The FEA models considered a semi-pipe configuration (Fig. 4), where the largest principal outer diameter and the eccentricity occur on the symmetry plane. The simulated pipe length was seven times the casing outer diameter, complying with specifications for physical testing (API TR 5C3, 2018; ISO 10400:2018, 2018).

The material properties of L80 steel used in the modelling were

determined experimentally, in laboratory tensile tests performed on round (rod-shaped) L80 test specimens with distinct notch radii (cf. Ruggieri, 2004). The strain-hardening response has been calibrated using an inverse method, thereby incorporating the large strain domain as occurring in the post-necking phase of tensile tests (Ling, 1996). Linear elastic material properties have been applied to the Local Expander tool. The simulations do not consider the effects of external cement or the surrounding casings and rock formations.

Radial extension and retraction of the Local Expander tool have been simulated by incrementing the axial displacement of the actuated cone, while axially fixing the set of expander fingers at the rear end position. The expander fingers are then forced out radially due to the contact definition between these members. For each pipe thickness, two expansion cases have been considered, where the extent of radial displacement was varied between 12.7 and 19.1 mm (cf. Local Expander tool max. radial increase, Table 1).

The burst and collapse simulations have been set up to simulate common laboratory testing conditions (API TR 5C3, 2018; ISO 10400:2018, 2018) of respectively capped-end, internal pressure and pure-external pressure loading conditions. These burst and collapse simulations use as starting condition the final geometry and distributions of (plastic) strains, strain-hardening and residual stresses resulting from the simulated expansion and the subsequent retraction of the Local Expander tool. The pressure has been applied incrementally until the maximum bearing capacity of the pipe was reached. The results were compared to reference FEA data, obtained by simulating burst and collapse testing of an undeformed L80 casing (i.e. a dent of 0 mm radial displacement), otherwise imposing the same pipe shape imperfections and burst or collapse loading conditions.

4.2.2. Laboratory testing of casing burst load capacity

In addition to the FEA modelling, physical testing was conducted to assess how the presence of LCE-induced indentations may impact casing burst strength. In the physical test, the response to internal pressurization of a dented casing was evaluated and compared to that of an undented but otherwise identical casing pipe. Two sections of 1.5 m length were cut from a single K55 casing (7″ OD, 23 lb/ft = 17.78 cm OD, 34.23 kg/m). After a 7″-model Local Expander tool was used to create a dent midway along one of them, both sections were capped off using welded steel flanges equipped with pressure line connections. Both pipes were uncemented and longitudinally unconstrained. Burst load capacity testing was performed in line with ISO 10400:2007 (API TR 5C3, 2018) practice, except for the pressure application rate, which exceeded 344.74 bar/min during the initial stages of testing for both samples. Pressurization was achieved by applying a constant pump rate, using equipment with a maximum operating pressure of 650 bar. Similar comparative testing was conducted on two 1.2 m sections of a T95 Type 1 casing (10-3/4″ OD, 73.2 lb/ft = 27.31 cm OD, 108.93 kg/m). Here, the dent was created using a mock-up expander head, similar to the 10-3/4″C-type (Table 1), actuated using a mechanical loading frame. The dented casing was locally expanded to an outer diameter of 309.3 mm. For testing of the T95 Type 1 casing sections (API internal yield pressure 695 bar), the experimental facilities were modified to allow higher pressures (1000 bar).

5. Field trial programme

To assess the effectiveness of the Local and Energetic Expander tools, a field-testing programme was implemented in the Canadian oil and gas development region known as Groundbirch, in Northeast British Columbia. A trial plan was presented to and approved by the local jurisdictional regulator, with testing in the first trial well, involving SCVF shutoff using the Local Expander tool, commencing in Fall 2018. In total, six wells were part of the initial field-testing programme of the Local and Energetic Expander tools. Per tool type, field testing was executed in two phases: Phase 1 consisted of a single well, Phase 2 involved two additional wells. For the Local and Energetic Expander tools, these test wells will be referred to as WLE-# and WEE-#, respectively. The two-phase testing strategy allowed time to interpret and analyse the initial trial results and improve the tool string configuration or intervention procedure prior to replication.

5.1. Regional geology and field development

The Groundbirch asset is located about 50 km south of Fort St. John, British Columbia. The field lies within the Western Canadian geological region known as the Peace River Region, situated at the western edge of the Alberta Plateau within the Interior Plains (Catto, 1991; Mathews, 1986), east of the Northern Rocky Mountains.

Shell's current field development strategy targets unconventional natural gas from the Lower Triassic Montney Fm., situated ~2500 m below the surface. Montney gas is trapped within an alternation of siltstones and shales, and is extracted through hydraulic fracturing of the formation. However, when Shell acquired the Groundbirch assets in 2008, the company also acquired an inventory of legacy exploration wells that target various formations and utilize a variety of well designs. These inherited legacy wells form the majority of Shell Canada's suspended well inventory. With an annual target of a 10% reduction in suspended well counts through decommissioning efforts, Shell has been actively working to improve understanding of the formations contributing to SCVF and the factors that contribute to successful and permanent remediation thereof.

Well designs vary, but commonly include a surface casing, landed below the base of useable groundwater (defined by the local regulator as groundwater with up to 4000 mg/L total dissolved solids, for the purpose of protecting potable water sources – BC Oil and Gas Commission, 2019) and cemented to surface, and a production casing, also generally cemented to surface. Trajectories are usually vertical in the zones of interest for wellbore seepage, although many wells are deviated or horizontal in the producing horizon. Fig. 5 shows generalised wellbore schematics, imposed on a simplified regional stratigraphy that indicates the formations commonly contributing to wellbore leakage and those used in caprock restoration efforts.

5.2. Field trial preparation and methods

5.2.1. Well selection and dent interval selection

All six trial wells were selected for testing based on the following characteristics:

- The base of groundwater protection is covered by surface casing and surface casing has been cemented to surface with no evidence of annular leakage (annular leakage outside of the surface casing is known as gas migration).
- The production casing has been cemented to surface, as established through primary cementing reports or logging data (in one case, the well was cemented to surface in a remedial operation).
- Above each potential source formation, there exists at least a 2 m interval of non-porous rock such as shale (defined below) and adequate bulk cement in which to place expander dents. Optionally, there is evidence of micro-annuli, suggesting the flow path of the SCVF gas is near-casing.
- Source formations are not sour, and not significantly over-pressured (under 11 kPa/m expected case pore pressure gradient).
- No known casing integrity issues exist, such as leaks or severe corrosion.

Note that the above criteria are not intended as rigid, permanent boundary conditions for application of LCE tools, rather they have been applied as a simplification tool for early field trials in order to minimize uncertainty and complexity when interpreting field trial results.

In preparation for each SCVF remediation job, an integrated subsurface

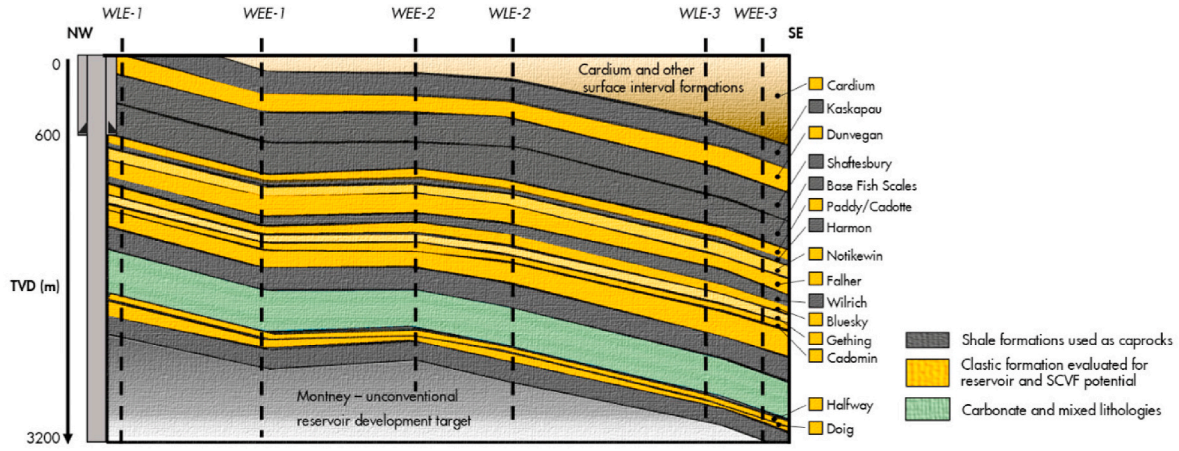

Fig. 5. Generalised stratigraphy cross-section, from the northwest to southeast, of the Groundbirch field, with common intervals of focus for sources and caprocks in SCVF remediation indicated. Internal shale breaks within intervals not represented at this scale. An idealised well schematic is given for WLE-1, representing the architecture commonly encountered in legacy wells, including those discussed in this paper. Note that the general stratigraphy dips towards the southeast, where the same formations are encountered deeper in the wells (approximate positions of the other five trial wells are indicated schematically, using dashed lines). Base of groundwater is covered by surface casing in all wells.

evaluation was performed to determine the probable source(s) of the SCVF gas. The factors considered in this evaluation include a full wellbore, formation by formation analysis of gas flow potential, making use of available log data to evaluate porosities and reservoir fluids, offset production data, and other indications of gas such as historical kicks or drilling mud gas, and a weighted ranking of the gas' geochemical match, based on carbon isotope data and composition ratios. These subsurface data were overlain with current and historical logs, such as cement bond logs (CBL), noise logs and neutron-density logs, as well as vent flow and pressure data. The result of this integrated analysis was a list of formations (typically one to three) that were interpreted to be the main contributors to the SCVF.

Intervention depths were selected on the basis of the following criteria:

- Presence of non-porous rock above the top porous package in the source formation (best available in the region of interest, targeting porosity <3%)
- Presence of sufficient cement and evidence for micro-annuli (near-casing defects), as indicated by an improved bond index on a 7 MPa pressure pass over a non-pressurised 0 MPa CBL.

5.2.2. Monitoring before, during and after intervention

Before commencing each intervention, a monitoring device capable of measuring the real-time flow rate and flowing pressure would be installed on the open surface casing vent. The vent flow monitoring device, called a Vent Nanny V3 (Roke Technologies, 2020), uses a positive displacement flow meter to measure the gas flow rate and pressure. A zero-flow measurement using this device indicates that the vent flow gas source is unable to produce enough pressure to overcome the back pressure exerted by the positive displacement flow meter, equal to 2.5 cm of water (~2.45 mbar). The device is thus designed to be functionally equivalent to the traditional bubble test, which is mandated by the local jurisdictional regulator and involves submerging the vent opening in 2.5 cm of water and counting bubbles over a 10-min period. The Vent Nanny V3 systems remained operational during and after the interventions, continuously logging vent flow rate. Standard 10-min bubble tests (Alberta Energy Regulator, 2003) were performed upon removal of the monitoring system. In addition to the vent flow measurements, post-intervention calliper and CBLs were obtained for the dented intervals of wells WEE-2 and WEE-3. The six trial wells were subsequently included in the Groundbirch annual SCVF monitoring summer programme.

5.2.3. Dent placement

Dents were placed in sets of three, completed in the order top-bottom-middle or bottom-top-middle, for both the Local and Energetic Expander tools. This placement strategy ensured the annular cement was axially constrained by the first two dents, allowing the middle dent to create a densifying effect. For the Local Expander tool, the dents in a set were spaced about 30 cm apart. For the single-shot Energetic Expander tool (EE-SS), the spacing was increased to 50 cm, as a mitigation against added depth uncertainty associated with placing dents in three separate runs. In the multi-shot Energetic Expander tool (EE-MS), three explosive charges, spaced 30 cm apart, were activated simultaneously.

For the Energetic Expander tool, reference tests using representative casing sections and conducted at representative pressures were performed to calibrate the amount of explosive needed to achieve the target casing expansions in the trial wells. Since the energetic expansion process is pressure-sensitive, a greater amount of explosive material would be required to achieve the same target OD, when setting dents deeper in a well. Based on reference tests using L80 casings (5-1/2″ OD, 17 lb/ft = 13.97 cm OD, 25.30 kg/m), a 106.7 mm OD Energetic Expander tool armed with 146 g of HMX explosive was used in the WEE-1 field trial to create dents across the deeper Wilrich Fm. For the shallower Base of Fish Scales, capping the Paddy-Cadotte Fms. source, and for surface casing isolation, 138 g of explosive was used. For the WEE-1 field trial, individual dents would be placed on separate wireline runs, with the tool remaining being pulled to surface and changed out after each dent. Casing size and weight were identical for the subsequent WEE-2 field trial. Accordingly, 138 g of HMX was used for both denting intervals, aiming to expand the casing to 164 mm OD across the bottom of the Shaftsbury shale Fm. and just inside the surface casing. In preparation of EE-MS deployment in the WEE-2 field trial, a reference test using three charges with 138 g of HMX explosive was performed. The expanded OD obtained using the EE-MS tool was 2 mm less compared to the single-shot configuration across all three dents. Additional testing was required for the WEE-3 field trial, using a L80 casing (7" OD, 26 lb/ft = 17.78 cm OD, 38.68 kg/m). Based on the results, a 144.8 mm OD Energetic Expander tool armed with 258 g explosive was used for all dent intervals on trial well WEE-3.

6. Laboratory and modelling results

6.1. Sealing performance studies

The functionality of the Local and Energetic Expander tools was assessed in a series of laboratory sealing tests, performed on full-scale samples representing intervals of cemented wellbore. The samples were made to contain structural defects such as micro-annuli, to simulate initial conditions of impaired zonal isolation. Bearing in mind that intact cement has a very low matrix permeability, typically in the range of 10^{-21} to 10^{-17} m^2 = 1 nD to 10 μD (Montgomery, 2006; Taylor, 1992), flow measured in the experiments likely occurred through these fractures and micro-annuli. However, to facilitate evaluation of the tools' performance, we will describe the transport properties of the samples (in both the initial and remediated state) in terms of their equivalent permeability, κ_{equiv} [m^2]. This equivalent permeability is calculated with respect to the length of the cemented section, L [m], and the cross-sectional area of the annular region between the casings, $A = \pi(R_{oc}^2 - R_{ic}^2)$ [m^2], where R_{oc} [m] is the inner radius of the outer casing and R_{ic} [m] denotes the outer radius of the inner casing. Following this definition, the transport properties of the samples can be directly compared to those of a hypothetical, perfectly bonded and cemented annulus section of equal dimensions, for which κ_{equiv} would approach the cement matrix permeability. The κ_{equiv} calculations are performed using standard formulations for compressible flow (e.g. Rushing et al., 2004) and fluid properties for dry N_2 gas (NIST SRD-69), according to the equation:

$$\kappa_{equiv} = \frac{2Q_m \mu RTL}{M\left(P_{us}^2 - P_{ds}^2\right)A}$$

Here, Q_m [kg/s] is the measured N_2 mass flow rate, μ [Pa s] is the dynamic viscosity, R [J/K mol] is the gas constant, T [K] denotes temperature, M [kg/mol] is the molar mass of N_2, and P_{us} and P_{ds} [Pa] denote the applied pressure upstream and downstream of the sample, respectively (note $\Delta P = P_{us} - P_{ds}$).

6.1.1. Dual annulus laboratory testing of the Local Expander tool

Evaluation of the Local Expander tool involved tests on a 1.48 m-long cemented section with dual annulus configuration (Fig. 3). The initial transport properties of the two cemented annuli were measured separately. Fig. 6a and 6b show N_2 flow rate versus applied pressure difference for the outer and inner annulus, respectively. In the outer annulus (OA), the measured flow rate increased linearly with imposed differential pressure and exceeded the equipment measurement limit (900 norm.ml/min) at differential pressures below 3 bar (Fig. 6a). This corresponds to κ_{equiv}-values in the range of 10^{-14} to 10^{-13} m^2 = 10 to 100 mD, reflecting a scenario of compromised zonal isolation (Fig. 6c). The inner annulus (IA) showed slightly more complex behaviour, with significant flow rates starting to register only upon application of differential pressures exceeding 30 bar, ultimately reaching 250 norm.ml/min at ΔP = 50 bar (Fig. 6b). This apparent pressure-threshold may reflect effects caused by the casings' elastic response to internal pressurization, e.g. hydraulic opening of micro-annuli, or might be related to progressive displacement of aqueous fluid originally present in the micro-annuli. In any case, these effects complicate evaluation of the initial equivalent permeability of the inner annulus. Disregarding the threshold in pressure and calculating κ_{equiv} per as described above yields values in the range of 10^{-17} to 10^{-16} m^2 = 0.01 to 0.1 mD (Fig. 6d), while estimates based on the slope in Fig. 6b give slightly higher values (10^{-15} m^2 = 1 mD).

At this point, a set of three dents was created using a 7″-model Local Expander tool. The impact on the sample's sealing integrity was subsequently evaluated in a second series of flow-through tests. For the inner annulus, application of differential pressures of up to 50 bar resulted in flow rates reaching roughly 10 norm.ml/min (Fig. 6b). This corresponds to an equivalent permeability of 10^{-19} to 10^{-17} m^2 = 0.1 to 10 μD (Fig. 6d). These values fall within the range of what can be expected from a 1.48 m-long section of well-bonded, defect-free cement, suggesting that the LCE process effectively restored zonal isolation in the inner annulus. Turning to the outer annulus, here the flow rate increased linearly with the applied differential pressure until it reached ~300 norm.ml/min at ΔP = 10 bar (Fig. 6a). This yielded an equivalent permeability in the order of 10^{-16} to 10^{-15} m^2 = 0.1 to 1 mD. While this does not constitute complete restoration of zonal isolation, the Local Expander tool thus accomplished a ten to hundredfold decrease in flow rate in the outer annulus. This effect was achieved due to partial transmission of the deformations and load applied to the inner pipe via the inner annulus cement. Placement of the fourth dent did not

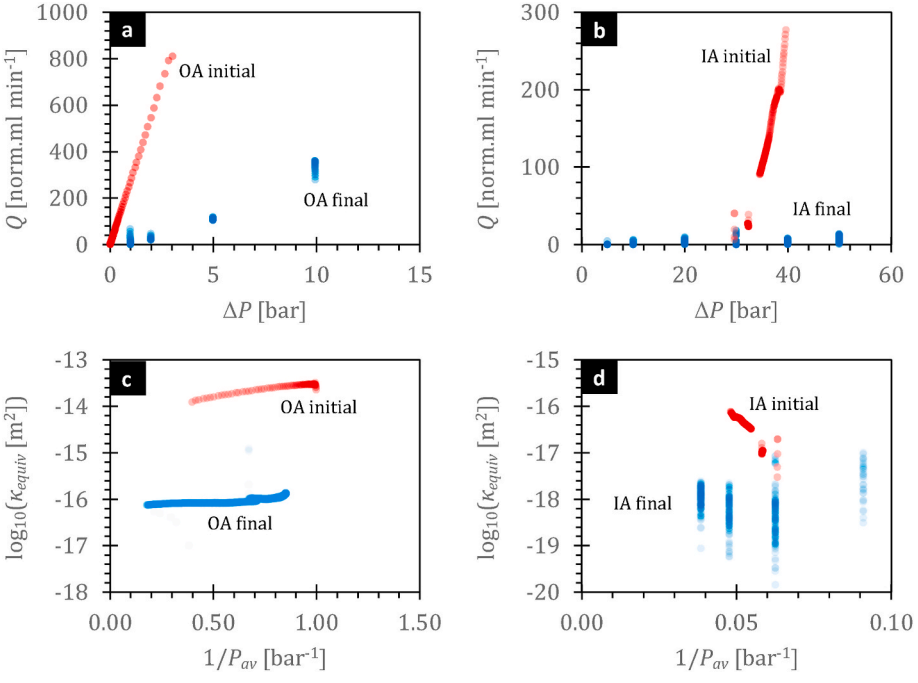

Fig. 6. Permeametry results of Local Expander tool test on dual annulus configuration, with plots of flow rate versus applied pressure difference for a) the outer annulus (OA) before and after expansion (denoted initial and final, respectively), and b) the inner annulus (IA) before and after expansion; plots c) and d) show the same data, expressed as equivalent annulus permeability, plotted against the inverse average pressure. Note IA attained an equivalent permeability in the range of typical cement matrix permeabilities, while the seepage rate in OA decreased about two orders upon casing expansion.

significantly improve the sealing performance of the outer annulus.

6.1.2. Laboratory testing of the energetic expander tool

The Energetic Expander tool was evaluated using a 1.3 m-long cemented sample containing 4-1/2″ and 7” OD casings (see Section 4.1.2). The initial transport properties of the cemented annulus were determined in a first zonal isolation test. Fig. 7 shows the applied pressure difference (ΔP) and resulting N_2 flow rate versus time. Flow rates clearly exceeding the noise level were observed after increasing the pressure difference across the sample to 0.5 bar. Application of $\Delta P = 1$ bar resulted in flow rates exceeding 250 norm.ml/min and flow continued to increase slowly during the next 2 h of measurement, without attaining steady state (Fig. 7a). This behaviour corresponds to an initial equivalent permeability in the order of 10^{-16} to 10^{-15} $m^2 = 0.1$ to 1 mD (Fig. 7b).

At this stage, Energetic Expander technology was deployed to create a single dent about midway the length of the cemented casing assembly. The degree of expansion was assessed by measuring the outer diameter of the 7” casing, which locally increased by up to 6.4 mm, i.e. ~3.6% OD increase. The expanded sample was then subjected to a second zonal isolation test, which showed the energetic LCE process had markedly improved the sealing properties of the cemented annulus (Fig. 7c). The initially higher flow rates (t <4 h) reflect the last stages of sample stabilization, where the measured flow rate is related to pressurization, rather than actual flow-through (recall that flow into, rather than out of the sample was measured). Applying ΔP of up to 50 bar, the resulting flow rates were transiently high, but then quickly fell and remained well below 5 norm.ml/min during stable measurement intervals (Fig. 7c). The corresponding stable equivalent permeability falls in the range of 10^{-20} to 10^{-19} $m^2 = 0.01$ to 0.1 μD (Fig. 7d), effectively reaching the lower measurement limit of the testing setup for samples of this length and size. These values rival the sealing capacity that could theoretically be expected from a 1.3 m-long section of perfectly-bonded, defect-free cement, indicating the LCE process effectively restored zonal isolation.

6.1.3. Effect on cement sheath structure

The impact of LCE-induced deformation on the physical properties of the cement sheath was evaluated by visual inspection and microstructural analysis of samples obtained from the cemented casing sections used in the sealing performance studies and other LCE tool performance tests. In the following, our general observations and main findings will be described on the basis of some illustrative examples from various experiments (Fig. 8).

Fig. 8a shows a window that was cut into a cemented annulus configuration, containing dents which were imposed using a prototype Local Expander tool. Although the window provides only restricted access to the internal structure of the sample, note this method helped preserve the mechanical integrity of the nested casings, allowing the cement sheath to be studied under (partial) residual stress-strain conditions that are more representative for downhole situations. The window exposed the inside of the inner casing, with two rings of rectangular toothmarks delineating the dent positions. The window also provided a radial section through the casing-cement-casing assembly. No fractures could be discerned in the cement sheath and the casing-cement interfaces appeared tight. The white patches that can be seen on the cement in Fig. 8a are mineral efflorescence, related to drying of the cement after cutting the window. Fig. 8b shows the pieces of cement and casing that were cut away in order to create the window. The cement retained its cohesion and could be retrieved in more or less one piece. Fig. 8c–d show XRCT images of the cut away cement sample, where a zone of increased X-ray attenuation (marked by lighter shades of grey) could be observed around the dent location in both radial and tangential views, indicating the density locally increased. During optical microscopy investigations, however, the microstructure of this densified, compacted zone did not show clear differences compared to the non-compacted cement (Fig. 8e–f). Fig. 8g shows a longitudinal cut through the casing-cement-casing assembly of another sample, where dents were created using a 7″-model Local Expander tool. Sealing

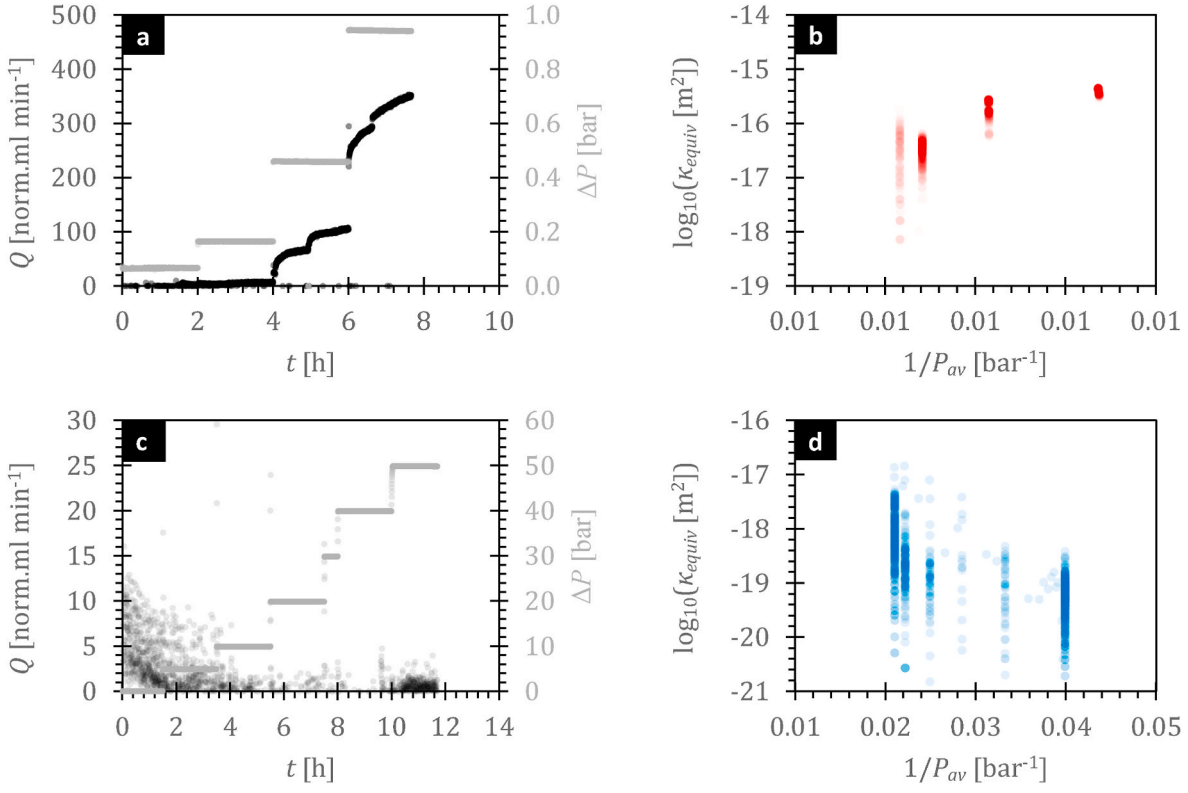

Fig. 7. Permeametry results of Energetic Expander tool test on cemented casing section, with a) initial flow through test results, showing flow rate and applied pressure difference with time, b) same date plotted in terms of the initial equivalent permeability of the cemented annulus, c) flow through test results after dent was created, d) equivalent permeability after dent was created.

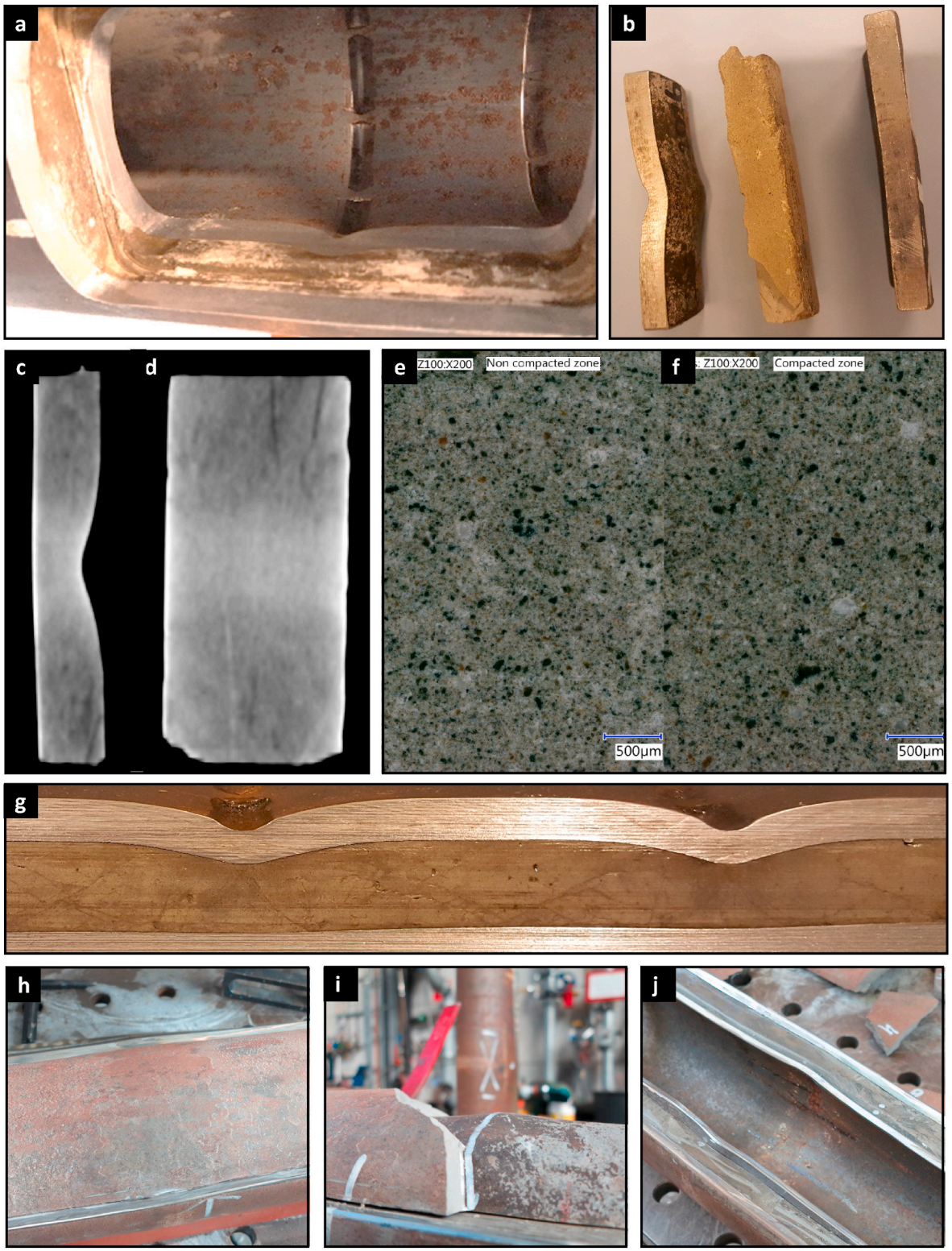

Fig. 8. Overview of microstructural observations, with a) photograph of window cut into casing bearing two dents created with a Local Expander tool, b) cement and casing elements recovered during creation of window, c) XRCT images of cement recovered from window, d) reflected light microscopy images of non-compacted and compacted cement, g) photograph of radial section through another Local Expander sample, h-j) show photographs of the sample used in the sealing performance test of the Energetic Expander tool (Sections 4.1.2 and 6.1.2).

performance testing of this cemented sample showed a reduction in the equivalent permeability down to cement matrix permeability values. Note Fig. 8g depicts a sample that was sectioned along its entire length, not a window into an otherwise intact cemented casing section. The cement sheath displayed multiple sets of shear bands, apparently emanating from dent locations. They were most clearly visible, as slightly darker lines, when the cut face of the cement started to dry out upon exposure to lab humidity. Possibly, these structures were more

apparent in this sample due to dilatation, which would have occurred as the confining stresses provided by the casings were released upon sample cutting. In any case, these shear bands seem to have accommodated deformation in the cement without significant loss of cohesion.

Fig. 8h–j shows photographs of the cemented casing sample used for the sealing performance test of the Energetic Expander tool, described in Sections 4.1.2 and 6.1.2. The photographs show how the sample is being taken apart after experiment completion. Fig. 8h depicts the outer surface of the cement sheath, after careful removal of the upper half of the outer casing. No fractures were observed upon visual inspection, but the outer surface of the cement sheath was clearly deformed, closely following the dented shape of the removed outer casing. When an attempt was made to remove the cement sheath from the inner casing pipe, this proved difficult to achieve around the dent location, especially compared to other parts of the cemented sample. Regrettably, our attempt to remove the cement sheath caused it to break before it came loose from the inner pipe (Fig. 8i). Fig. 8j shows a longitudinal cross-section through the opposite half of the sample. Upon visual inspection, the cemented annulus appeared to be free of fractures and have tight interfaces.

6.2. Casing integrity studies

6.2.1. Finite element modelling of the casing indentation process

The denting of casing pipe using a Local Expander tool is a complex deformation process, which will here be illustrated for the case of a perfectly cylindrical pipe, where cyclic symmetry (due to finger arrangement) conditions have been utilised. Fig. 9 shows two stages during the deformation process in a longitudinal section through the pipe and an expander finger. The main straining of the pipe occurred in the hoop (circumferential) direction and was associated with the imposed radial displacements. The hoop straining was largest at the crest of the dent. As the finger was forced outward more, a larger portion of the casing adopted the curvature of the finger crest through bending effects. Bending effects, with opposite sign of the curvature, also occurred in the transition zone between the pipe and the dent. Here, the pipe was not supported by the finger and material got displaced by transfer or internal tension, shear and bending loads.

Fig. 10 shows a section through the crest of the expander finger during various stages of the expansion process (still under cyclic symmetry conditions). As radial displacement of the fingers increased, gaps opened-up between the neighboring fingers, causing an increasing portion of the pipe inner circumference to lose contact with the fingers. Consequently, the degree of plastic staining became non-uniform around the pipe circumference. The degree of wall thinning became somewhat less at the unsupported sections. A zone of increased plastic straining in the pipe occurred along the edge of the fingers. This zone is associated with plastic relief of (contact) stress-concentrations.

Fig. 11 shows the final distributions of equivalent plastic strain and the residual von-Mises stress after the Local Expander tool has been retracted. In this simulation, an L80 casing pipe (9-5/8" OD, 47 lb/ft = 24.45 cm OD, 69.94 kg/m) with initial ovality and wall thickness imperfections incorporated, was dented to 12.7 mm radial displacement. In addition to the expander finger induced cyclic variations, the overall strain level increases from bottom to top. This is attributed to the applied non-uniform wall thickness in the initial pipe geometry, which further developed during the expansion process. Apart from some 'finger induced hot-spots' the highest overall residual stresses occur in the transition zone from the nominally straight pipe to the dent.

6.2.2. Finite element modelling of casing collapse failure

The collapse strength of pipes refers to the load bearing capacity of the pipes under predominant external pressure loading conditions. It is governed by the stability of the nominally-round pipe shape. Fig. 12 shows the calculated responses of L80 casing pipes (9-5/8" OD, 47 lb/ft = 24.45 cm OD, 69.94 kg/m) to collapse loading, plotting pipe ovality versus applied external pressure, for undented pipe as well as dented pipes with 12.7 and 19.1 mm applied radial displacement. Response curves for dented pipes are given for both the main pipe body (represented by a position half-way between the dent and pipe end) and for the crest of the dent. Note the denting process reduced the initial pipe ovality locally around the dent. Moreover, upon collapse loading, ovality in the pipe body developed at a slower pace with pressure in the dented pipes, compared to the undented reference pipe. Further note that the ultimate pressure bearing capacity also increased when dents were applied (Fig. 12). Qualitatively the same effects were observed for the thinner and thicker pipe cases considered in the simulations. Given these results, the dents seem to serve effectively as local stiffener against collapse failure. Note, however, that this will practically no longer be effective for larger pipe lengths. The conclusion from these analyses is therefore that collapse strength of dented pipes remains to be governed by the pipe body, with dents possibly acting as local stiffeners.

6.2.3. Finite element modelling of casing burst failure

The burst strength of a pipe refers to its load bearing capacity under predominant internal pressure conditions. One of the design objectives is to prevent release of fluids contained inside the pipe to the environment. This involves the occurrence of yielding, plasticity and finally fracture of the pipe. Fig. 13 shows a capped-end example of the calculated changes in average diameter and minimum wall thickness that occur during internal pressure loading. The results shown are for a L80 casing (9-5/8" OD, 47 lb/ft = 24.45 cm OD, 69.94 kg/m) that has been dented to 19.1 mm radial expansion. Response curves are given for the pipe body, at a position halfway between the dent and the pipe end, and for the crest of the dent (note the latter curves exclude dimensional changes incurred during the denting itself). The response of an undented reference pipe is also shown. The diameter and wall thickness responses for the body of the dented and undented pipe were practically the same. The outer diameter increased ('ballooned') and wall thickness decreased under the applied internal pressure. The responses for the pipe body were linear up to the yield initiation pressure (here 618 bar, Fig. 13), where yielding initiated at the inside of the pipe body. In conventional

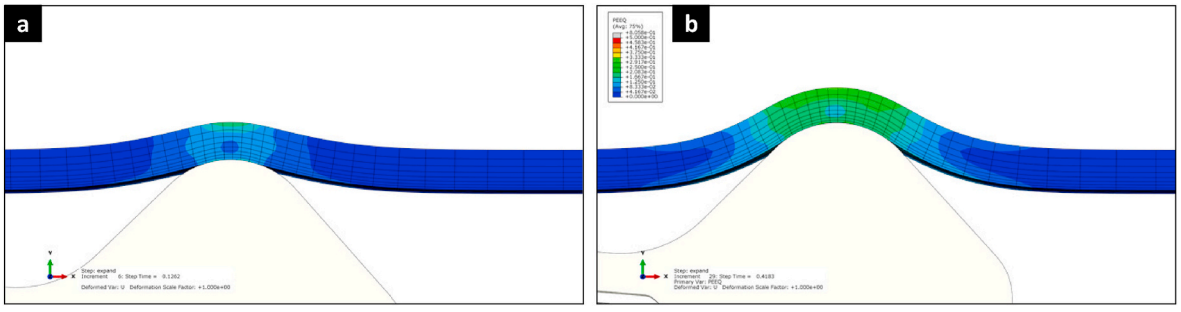

Fig. 9. Pipe deformation at various stages of the expansion process (longitudinal section, equivalent plastic strain as field variable), where in a) and b) the expander finger has been extended by 40% and 60% of its maximum, respectively.

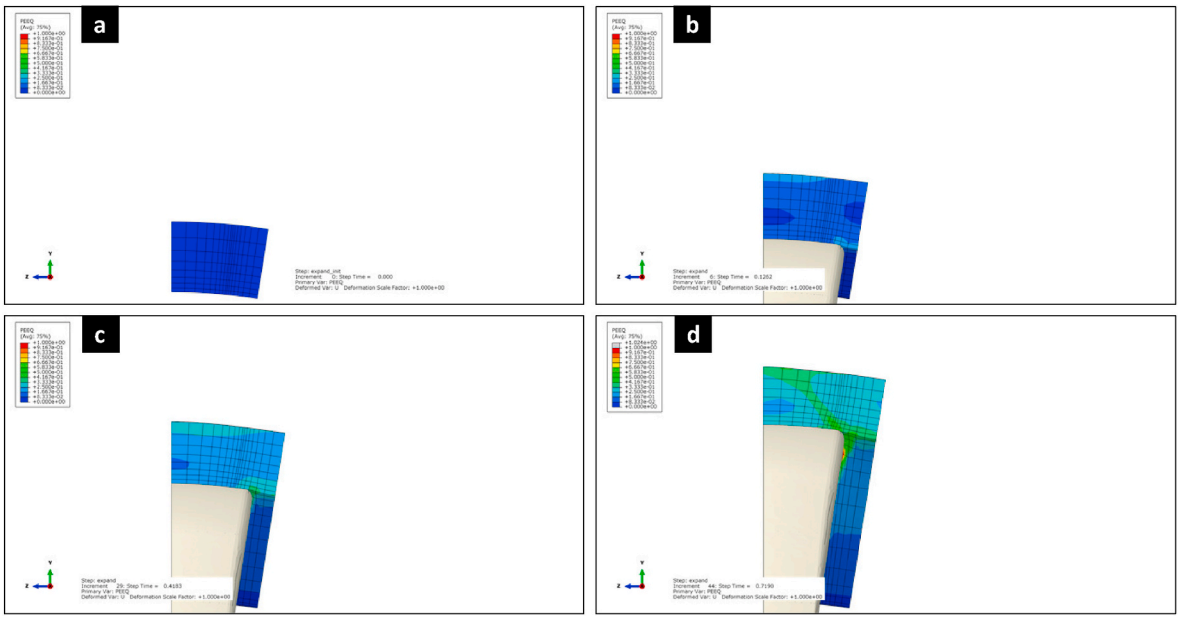

Fig. 10. Pipe deformation at various stages of the expansion process (transverse section, equivalent plastic strain as field variable), where a) shows the undeformed case, and b-d) progressively more extension, up to 80% of the tool maximum.

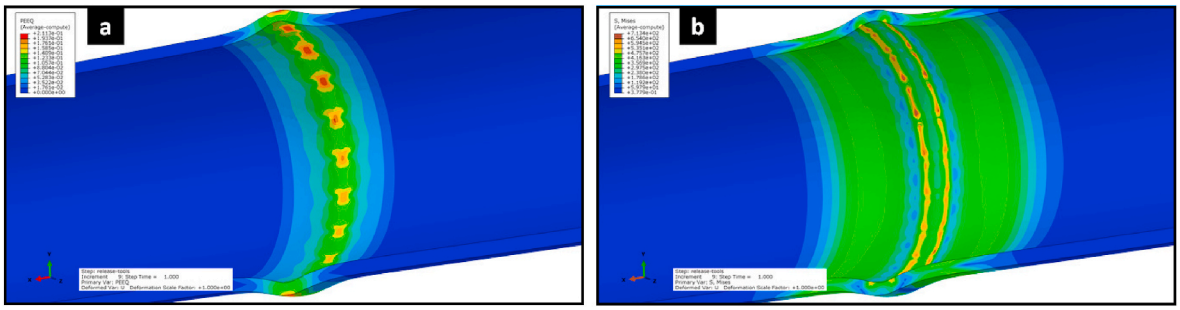

Fig. 11. Non-uniform plastic strains (a) and residual von-Mises stresses (b) due to initial wall thickness variations of the pipe and due to the finger configuration of the Local Expander tool. The simulation shown involves a L80 (9-5/8″ OD, 47 lb/ft = 24.45 cm OD, 69.94 kg/m) pipe that has been dented by up to 12.7 mm of radial displacement.

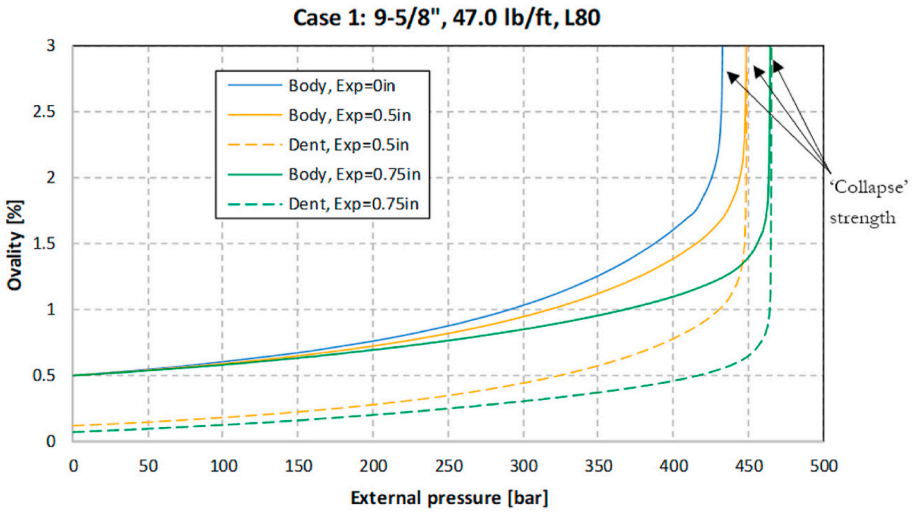

Fig. 12. Evolution of the ovality at the pipe body and at the crest of the dent versus the applied external pressure for an L80 casing pipe (9-5/8″ OD, 47 lb/ft = 24.45 cm OD, 69.94 kg/m) and for different degrees of applied denting. The pipe has initial imperfections of 0.5% ovality and 10% local wall thickness reduction.

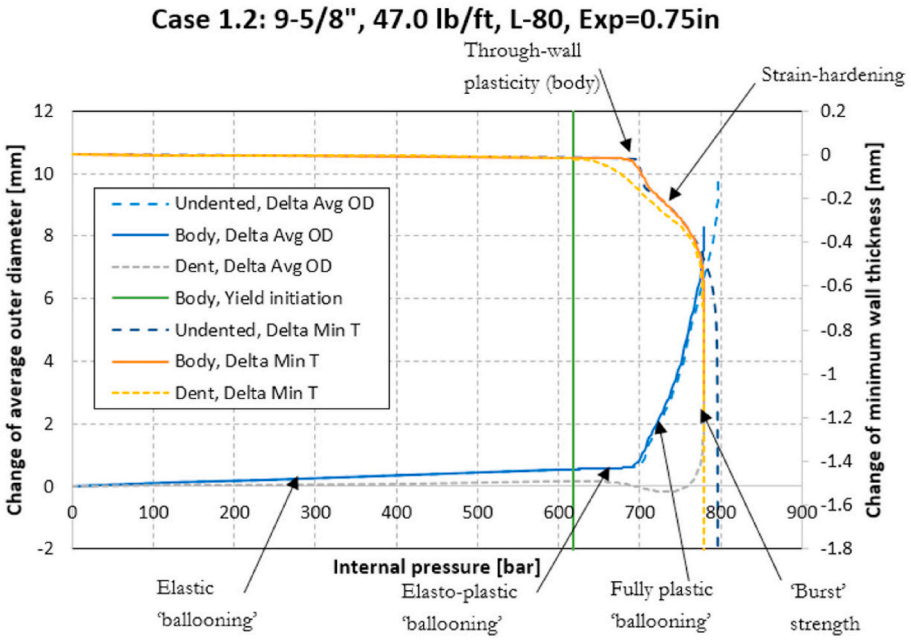

Fig. 13. Typical response of the changes of the average outer diameter (denoted Avg OD) and the minimum wall thickness (denoted Min T) versus internal pressure. The response curves are given for the pipe body and dent crest locations.

casing design practice, this pressure level or loading condition is used as the design limit. This internal pressure level can also be accurately predicted using industry accepted triaxial design equations (e.g. API TR 5C3, ISO 10400), when the minimum wall thickness of the pipe is accounted for. These conventional design equations assume the pipes have negligible residual stresses from the manufacturing process. It should be noted, however, that the pipe has significant capability to take additional loads beyond this initial yielding (Fig. 13). While the general design philosophy is to not exceed the yield limits, it is useful to discuss the post-yielding responses observed, as this provides insight in the actual safety margins with respect to events of (catastrophic) pipe failure and consequently losing the ability to contain pressure and fluids. It is of key importance to know whether these limits have been affected by the LCE-process.

After exceeding the yield limit, deformation of the casing became elastoplastic. With increasing internal pressure, the plastic zone, initiated at the inner surface of the pipe wall, grew at the expense of the zone in the pipe wall that still deformed elastically. However, (hoop) strains at the pipe outside remained elastic and thus small. Consequently, radial displacements, wall thickness reductions and pipe diameter enlargements also remained relatively small during this phase. Once plasticity occurred over the entire wall thickness (here 700 bar, Fig. 13), increasing rates of plastic ballooning and wall thinning occurred in the pipe body. Initially, strain-hardening of the material required progressively higher pressures for plastic deformation to continue. This effect levelled out, however, due to the opposing effects of material strain-hardening and continued wall thickness reduction. The ultimate pressure bearing capacity was reached at 778 and 796 bar for the dented and undented pipe, respectively (Fig. 13), as the weakening effect of pipe wall thickness reduction becomes dominant over strain-hardening effects. At this point, a necking zone occurred along the longitudinal direction, with accelerated plastic straining and stress-triaxiality development, with fracture being imminent.

As discussed in Section 6.2.1, the LCE denting process created large residual stresses in the pipe around the transition zone between the dent and the pipe body (Fig. 13). During burst loading, the presence of these residual stresses caused plasticity to re-initiate already at relatively low levels of applied internal pressure. These plasticity effects do not constitute a significant reduction of the load bearing capacity of the pipe as a whole, as the residual stress state is self-contained, i.e. does not have some net-resultant force. Therefore, these plasticity effects only constitute a plastic relief of the residual stresses.

Fig. 13 also shows that through-wall plasticity initiated at a lower pressure around the dent compared to the main pipe body. This weakening was related to an already reduced local wall thickness (note the material also already had undergone strain-hardening) and a different loading situation (e.g. also tension and bending effects). Therefore, on the one hand, the dent can be considered as a local weak spot. On the other hand, the body and dent responses (for a dented pipe case) both tended to the same limit pressure of 778 bar (Fig. 13). Hence, at a certain stage, local wall thinning around the dent can only develop further, or become unstable, if through-wall plasticity is also occurring in the overall pipe body. These results can be explained by considering the axial extent of the thickness reductions at the (crestal) position of the dents. Notably, the (tangential) displacement field should also be continuous in the axial direction of the pipe. Large gradients therein would involve large tangential and axial shear strains and associated stresses in the transition zone between the dent and main pipe body. This is energetically unfavourable and, therefore, the pipe body material adjacent to the dent effectively gives support to resist localized neck development at the dented zone. Still, the adjacent pipe body material does not act as a complete arrestor of necking at the dent. The dented zone remains to act as weakening, but the effect on the ultimate pressure bearing capacity (by induction of unstable necking) is very limited.

Qualitatively the same results were obtained for the other cases considered in this study involving thicker and thinner pipes and/or with the expansion of only 12.7 mm. The reduction of the ultimate pressure bearing capacity for the L80 casings considered in this study was within 10 and 30 bar when expanded to 12.1 mm and 19.1 mm radial enlargement, respectively. Overall, these are relatively small effects.

6.2.4. *Laboratory testing of casing burst load capacity*

The impact of LCE on the burst strength of the casing was also evaluated through physical pressure testing of dented and reference pipe sections. For the K55 casings (Fig. 14a), the dented and reference casing show very similar behaviour, with both pipes displaying more or less linear increase in pressure up to about 480 bar, after which a period of water injection at nearly constant pressure is observed. Upon continued

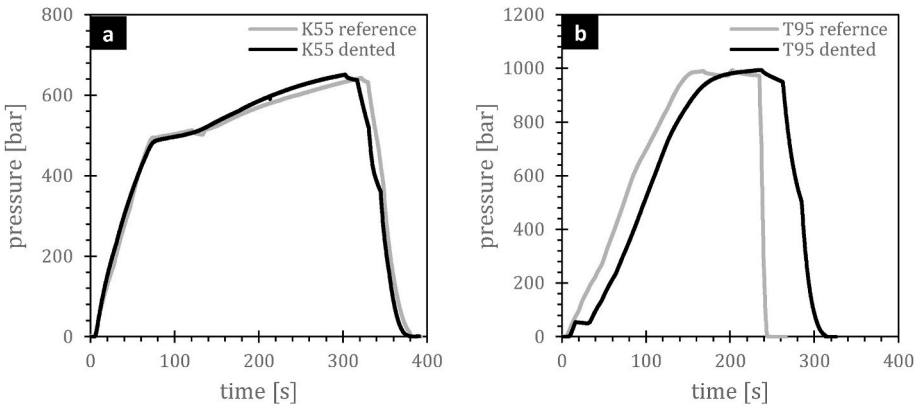

Fig. 14. Burst load capacity results for a) K55 (7″ OD, 23 lb/ft) casings and b) T95 Type 1 (10-3/4″ OD, 73.2 lb/ft) casings, with data for dented casings in black and reference (undented) casings in grey.

injection, the pressure gradually increases to 650 bar, the pressure limit of the test equipment used, thus warranting termination of the experiment prior to achieving burst. The dented and reference sections of T95 Type 1 casing likewise show essentially the same behaviour (Fig. 14b), where the pressure-time curves start to deviate around 900 bar for both pipes. Outer diameter measurements of the dented T95 Type 1 casing before and after pressure testing show that plastic deformation occurred mainly at positions P2 and P4, i.e. adjacent to the locally expanded interval (Table 2). Pipe burst was not achieved due to equipment limitations.

7. Field trial results and learnings

7.1. Local Expander tool field trials

7.1.1. Local Expander well 1 (WLE-1): November 2018

The first well selected for field trial of the Local Expander tool (WLE-1) is a vertical well located in the Northwest Saturn region of the field. It consists of 9-5/8" = 24.45 cm OD surface casing, landed at 440 mKB, and a 7" = 17.78 cm OD L80 grade production casing, landed at 2182 mKB. Casing weight varies but was 23 lb/ft = 34.26 kg/m across the interval of interest. The SCVF rate from this well varied seasonally, with a highest rate reported in five years of monitoring at 505 L/day, while the flow rate immediately prior to intervention was ~310 L/day (Fig. 15a).

Based on the integrated subsurface evaluation for WLE-1, three intervals were selected for localized casing expansion, namely: 1) a shale interval above the top porous package in the Notikewin Fm. (Fig. 5), with a set of dents located ~509 mKB, 2) the Falher caprock, for the potential source Bluesky Fm. (one set of dents at ~570 mKB and a second set at ~607 mKB), and 3) a final set of dents inside surface casing as a mitigation against shallow biogenic gas.

The intervention on WLE-1 was completed over a period of two days, 24–25 November 2018. Execution of the field trial was an operational success, with no tool challenges or delays. During the intervention, the flow rate increased slightly, which may have been a result of pressure test cycles on the casing (Fig. 15a). The flow subsequently decreased from an average of 310 L/day to effectively zero in 12 days. Note this downward trend did not begin until after the intervention had been completed, in fact not until after final pressure testing of the wellbore (at 7 MPa for 10 min) on 25 November 2018. For this reason, it was not possible to infer which set of dents contributed in what capacity to the observed decrease. Note the flow rate showed characteristics of exponential decay, suggesting the source had been isolated and the slow decline represented gas column bleed-off (Fig. 15a).

On 13 December 2018, the vent flow meter was closed off to allow build-up of pressure. According to Canadian regulations and standard industry practice, the pressure is considered stabilised if it changes less than 2 kPa/h over a 6-h period (Alberta Energy Regulator, 2003). The stabilised pressure build-up before intervention was 715 kPa. The pressure build-up on 13 December 2018 reached a stabilised value of 14 kPa in 24 h, and flowed briefly after opening the valve to flow mode (Fig. 15a). The flow rate returned to zero within two days and the total gas flow from the vent during this 48-h period was 11.3 L. This small volume likely indicates that the trapped annular gas was not yet fully bled off, even though the flow rate had been below the detection threshold of the measuring device for five days. The monitoring system was left running in open flow mode until 3 January 2019 and did not register any additional flow (Fig. 15a). At the time of removal, a 10-min bubble test was conducted with a result of no flow. Follow-up tests in the Summers of 2019 and 2020 yielded the same result: no flow in 10 min.

7.1.2. Local Expander well 2 (WLE-2): May 2019

WLE-2 is a vertical well drilled and completed in 2007, located in the south-central region of the Groundbirch field. It has 9-5/8" = 24.45 cm OD surface casing landed at 467 mKB, which was cemented successfully with returns to surface. An L80 production casing (7" OD, 23 lb/ft = 17.78 cm OD, 34.23 kg/m) was landed at 2818 mKB and also cemented successfully with returns to surface. WLE-2 was completed in and produced from both the Montney and Doig Fms. The well did not have a record of a surface casing vent flow until the time of abandonment, July 2016, when a bubble test yielded 40 bubbles in 10 min. The downhole zonal abandonments of the two producing formations were completed as planned, and a CBL was run to prepare for future SCVF remediation. After the 2016 zonal abandonment, the SCVF of WLE-2 was monitored annually, with a highest recorded flow rate of 880 L/day and highest stabilised pressure build-up of 68 kPa.

The integrated subsurface evaluation for WLE-2 resulted in a combination of multiple potential sources: 1) low-temperature, thermogenic fracture gas from the Base of Fish Scales, 2) minor contribution from the Paddy Fm. and 3) minor shallow biogenic methane gas. Additionally, CBL analysis indicated inadequate cement quality to achieve hydraulic isolation between the porous Notikewin and Fahler Fms. It was determined that cement coverage was sufficient to attempt to achieve

Table 2
Outer diameter measurements of dented T95 Type 1 casing before and after burst load capacity testing. OD = outer diameter; *estimated on the basis of P1 and P5 measurements.

Position	P1	P2	P3 (dent)	P4	P5
OD before burst testing [mm]	274.9 ± 0.2	274.6 ± 0.5*	309.3 ± 0.7	274.6 ± 0.5*	274.3 ± 0.5
OD after burst testing [mm]	275.3 ± 0.3	277.2 ± 0.3	308.8 ± 0.5	276.8 ± 0.4	275.2 ± 0.1

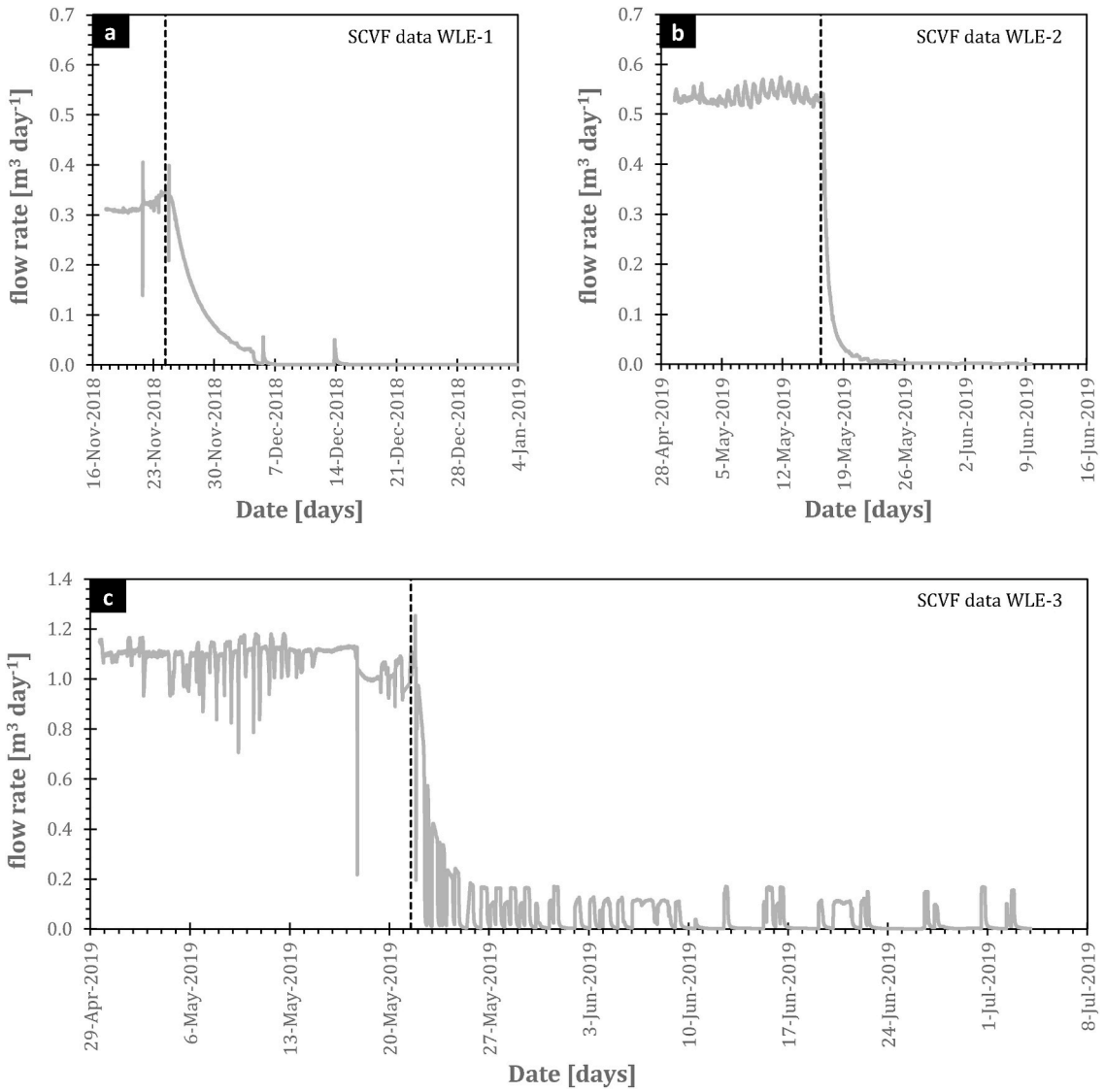

Fig. 15. Surface casing vent flow monitoring data prior to, during and after interventions using the Local Expander tool, with logged flow rate [m^3 day^{-1}] versus time [date] data for a) WLE-1, b) WLE-2, and c) WLE-3. Vertical, black dashed lines denote the moment at which Local Expander remediation procedures commenced. See main text for detailed descriptions.

hydraulic isolation using the Local Expander tool, rather than with a traditional cement squeeze. Accordingly, sets of dents were planned 1) across the interval between Notikewin and Falher Fms., to obtain hydraulic isolation between these formations, 2) near the bottom of the Base of Fish Scales, for the Paddy Fm. source, 3) near the top of the Base of Fish Scales, to address Base of Fish Scales fracture gas, and 4) inside the surface casing, for the shallow biogenic gas contribution.

Intervention on WLE-2 was completed on 16 May 2019. The sets of dents were placed using the Local Expander tool as planned, starting with the deepest interval and progressively moving upward in the well, to finish the last dents inside the surface casing. The vent was left in flow mode for the duration of the intervention, continuously logging flow rate (Fig. 15b). Once again it is not possible to infer which set of dents contributed in what capacity to the vent flow reduction, as the decline in flow began ~2.5 h after all dents had been placed. The main decline in flow rate appears to correlate with the start of a swabbing operation on the well, and the flow decelerates rapidly after swabbing, when the well was re-filled and pressure-tested to 7 MPa for 10 min. Overall, the flow rate went from an average of 530 L/day immediately prior to intervention to effectively zero flow in 20 days (Fig. 15b). The monitoring system was removed on 9 June 2019 and a regulatory bubble test was conducted, yielding zero bubbles.

7.1.3. *Local Expander well 3 (WLE-3): May 2019*

WLE-3 is a vertical well, drilled in the south Brassey region of the field in 2005 and completed in the Cadomin, Halfway and Doig Fms., with the objective of evaluating those zones for future development. It has 9-5/8" = 24.45 mm OD surface casing, landed at 464 mKB, which was cemented successfully with returns to surface. An L80 production casing (7" OD, 26 lb/ft = 17.78 cm OD, 38.69 kg/m) was landed at 2923 mKB and also cemented successfully with returns to surface. Prior to hydraulic fracturing, a 10-min regulatory bubble test was conducted and it was reported that the well did not have SCVF. After fracturing and flow testing the two shallower formations (Cadomin and Halfway Fms.), cement squeezes were performed into both intervals. Afterwards, the deeper Doig Fm. was hydraulically fractured, flow tested, and put on production for a one-month period. The well was subsequently shut-in long term and eventually suspended in 2011. The well did not have a record of SCVF until the time of abandonment, in July 2016, when a 10-min bubble test yielded too many bubbles to count. It was observed at this time that the SCVF would die off when 7 MPa pressure was applied to the wellbore and return when that pressure was bled off, indicating

the presence of a micro-annulus between the casing and the cement, which could be closed off by ballooning the casing. The downhole zonal abandonments of the producing formation and two cemented intervals were completed as planned, and a CBL was run to prepare for future SCVF remediation. After the 2016 zonal abandonment, the SCVF was monitored annually, with a highest recorded flow rate of 1157 L/day and stabilised pressure build-up of 1063 kPa.

The source identification process for WLE-3 resulted in an interpreted SCVF source mixture of ~80% Paddy Fm. gas and ~20% shallow biogenic methane gas from the Dunvegan Fm., similar to well WLE-2. CBL analysis indicated no additional remediation was required for hydraulic isolation between porous intervals. As such, dents were placed 1) near the bottom of the Base of Fish Scales for the Paddy Fm. source, 2) at the bottom of the Kaskapau Shale and 3) inside the surface casing, for shallow biogenic gas contributions from the Dunvegan Fm. All selected intervals had a measurable improvement in cement bond index on a 7 MPa pressure pass CBL over a 0 MPa pass CBL, suggesting micro-annulus development.

The intervention on WLE-3 was completed on 21 May 2019. All dents were placed as planned, starting with the deepest interval and moving upward to finish inside the surface casing. The flow rate immediately prior to the intervention averaged 1100 L/day, with significant fluctuations that apparently correlate with daily temperature changes (Fig. 15c). Given these fluctuations in flow rate before and during the intervention, it is not possible to ascertain how each set of dents contributed to SCVF reduction. After the intervention, the flow rate declined quickly and increasingly long times between surges of flow could be observed. After the first five days of rapid decline in flow rate, the flow rate started fluctuating between ~165 L/day and 0 L/day, with a flow surge every 3–4 days. Over time it became evident that the amount of time in between surges was increasing, indicating that the annulus was possibly liquid loaded and additional time would be required for a full bleed-off of entrapped gas. Over the last 10 days of monitoring, the vent flow rate averaged 20 L/day (Fig. 15c). After an extended monitoring period, the monitoring system was removed on 4 July 2019. At this time, a regulatory bubble test was conducted, and although zero bubbles were observed, it is clear that the flow was intermittent, rendering a 10-min test inconclusive.

7.2. Energetic expander tool field trials

7.2.1. Energetic expander well 1 (WEE-1): June 2019

The first field trial of the Energetic Expander tool was performed in WEE-1, a vertical well drilled and completed in 2000 in the north west Saturn region of the field. The well consists of a 8-5/8" = 21.91 cm OD surface casing, landed at 457 mKB, and a IK-70 grade production casing (5-1/2" OD, 17 lb/ft = 13.97 cm OD, 25.3 kg/m), landed at 2746 mKB, both cemented successfully with returns to surface. WEE-1 was completed in the Montney, Gething, Halfway and Bluesky Fms. The three shallower perforations were cemented in 2001. SCVF was first recorded in 2006. The deeper Montney Fm. was hydraulically fractured, and the well continued to produce from the Montney Fm. with a packer completion until suspension in 2013. At the time of suspension, a regulatory bubble test indicated too many bubbles to count. Well abandonment was initiated in May 2019, with a plug and cement zonal abandonment of the Montney Fm. (Fig. 5), followed by 0 MPa and 7 MPa pressure pass radial cement bond logging. At the time of suspension, this well became part of an annual field-wide SCVF monitoring program. Between 2013 and 2018, the highest recorded flow rate and stabilised pressure build-up were 4968 L/day and 3167 kPa.

The integrated subsurface evaluation for WEE-1 indicated probable gas sources in the Paddy-Cadotte and Bluesky Fms. Unlike other wells in the region, geochemical analysis did not indicate a contribution from shallow biogenic gas. CBL analysis indicated no additional remediation was required for hydraulic isolation between porous intervals. For the deeper potential source Bluesky sandstone, a target dent interval was selected near the bottom of the Wilrich shale, which serves as a caprock for the Bluesky Fm. Cement quality in the region of interest was consistent with no evidence of micro-annuli. As such, the dent interval was chosen 2 m above the Wilrich-Bluesky contact, in order to stop the gas flow as close to the source as possible. For the potential source Paddy-Cadotte Fms., the intervention depth was chosen near the bottom of the Base of Fish Scales shale which caps the Paddy Fm. An additional set of dents was selected near the bottom of surface casing, as a final isolation.

The intervention in well WEE-1 was executed as planned on 25–27 June 2019. The flow rate immediately prior to the intervention averaged 6315 L/day, with daily fluctuations with temperature change between 6000 and 6600 L/day, which was notably higher than any flow rate previously recorded for this well (Fig. 16a). Because the intervention was completed over a period of three days, WEE-1 was the first LCE field trial where it was possible to assess the flow-reduction impact of each individual dent interval. Fig. 16b shows flow rate recorded during the intervention and immediately after, including timestamps for each dent placed. From the real-time flow data, it appears the set of dents created in the Wilrich Fm. did not have any immediate impact on the SCVF rate. A declining flow rate trend was observed after a set of dents was placed in the Base of Fish Scales to address the Paddy-Cadotte Fm. potential source. However, this initial decline appears to have started levelling out before placement of the surface casing dents. Flow rate reduced notably after placement of dents inside the surface casing. These observations suggest the Bluesky Fm. was not significantly contributing to the SCVF. With the Paddy-Cadotte Fm. as likely source of SCVF gas, either the dents inside the surface casing trapped the Paddy-Cadotte Fm. sourced gas, preventing further bleed-off, or a shallow zone above the Paddy Fm. was serving as storage zone. Given this result, and the perceived risks of trapping source formation gas at the surface casing shoe and masking possible cross-flow between formations, a decision criterion was developed for subsequent LCE interventions, in which formation pressure and gas gradients for all intervention depths in a wellbore would be evaluated against fracture gradient of each shallower intervention formation, including the surface casing shoe, prior to determining if additional time would be required between dent intervals.

From 28 June to 4 July 2019, data was not recorded due to heavy rains causing flooding on the wellsite. When data collection was restored on 4 July, the flow rate was fluctuating, initially between 2 and 78 L/day with daily temperature variations, and less frequently over time. The average flow rate over the last ten days measured 24 L/day. When the vent flow monitoring device was removed on 28 July, zero bubbles were observed in the 10-min regulatory test. A follow-up bubble test was conducted on 6 October, again with zero bubbles. However, similar to WLE-3, this cannot be considered conclusive, given the fluctuating nature of SCVF on this well.

7.2.2. Energetic expander well 2 (WEE-2): November 2019

WEE-2 is a vertical legacy well in the northeast Sunset region, drilled in 2005 and originally completed in the Doig Fm., then later re-completed in the deeper Montney Fm. Both the surface casing (8-5/8" = 21.91 mm OD, landed at 404 mKB) and the L80 production casing (5-1/2″ OD, 17 lb/ft = 13.97 cm OD, 25.3 kg/m; landed at 2535 mKB) were cemented successfully with full returns reported. Several bubble tests were conducted throughout the well's life, indicating no SCVF. In 2016 the well was zonally abandoned and at this time a failed bubble test was reported. Follow-up inspections indicated variable flow from the surface casing vent. From 2016 to 2018, the highest flow rate recorded was 297 L/day, with a largest stabilised build-up pressure of 209 kPa.

The source identification process indicated the gas was of low thermal maturity, originating from the Base of Fish Scales and Shaftsbury Fm., with ~10% biogenic gas from the Dunvegan Fm. just below the surface casing shoe. While the Base of Fish Scales is generally considered a caprock in the region and does not have evidence of reservoir development or porosity, in this particular well gas is present on the log

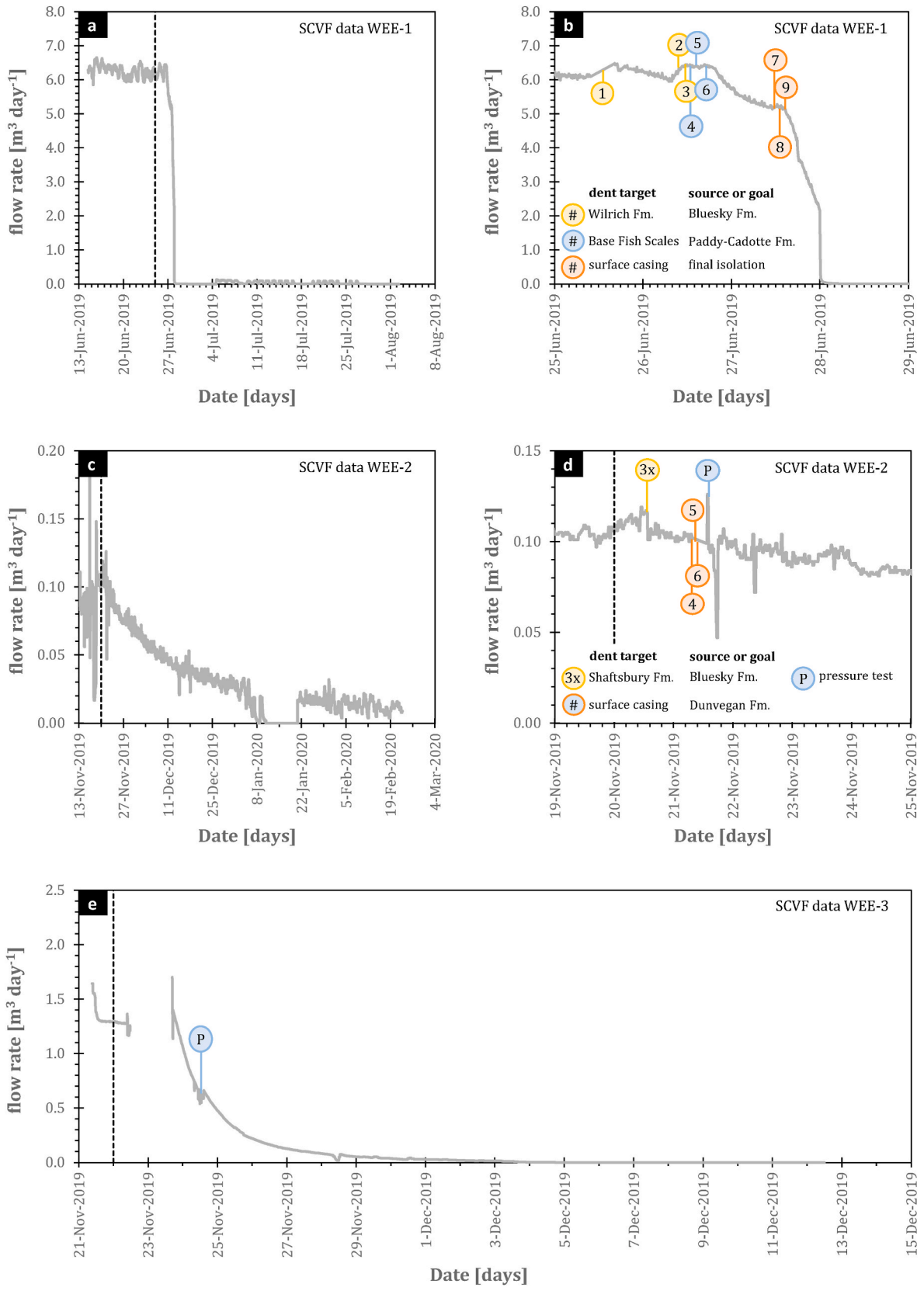

Fig. 16. Surface casing vent flow monitoring data obtained prior to, during and after interventions using the Energetic Expander tool. Flow rate [m^3 day^{-1}] versus time [date] data for a) WEE-1, b) detail of WEE-1, showing the timing of individual dents, c) WEE-2, d) detail of WEE-2, showing the timing of EE-MS deployment (denoted 3x) and subsequent individual dents, as well as timing of a post-intervention pressure test, e) WEE-3 data, with timing post-intervention pressure test indicated. Vertical, black dashed lines denote the moment at which Energetic Expander intervention procedures commenced. See main text for detailed descriptions.

analysis and the SCVF sample was a match for the formation's isotope fingerprint, which suggests probable fracture gas. Accordingly, dent intervals were targeted in the bottom of the Shaftsbury shale Fm. above the Base of Fish Scales, and just inside the surface casing to address the shallow biogenic gas contribution. Both intervals were selected in regions with overall good cement coverage and evidence for a near-casing micro-annulus. Building on learnings from the WEE-1 field trial, the pressure gradient of each contributing source formation was evaluated against the fracture gradient at the shallowest intervention depth near the surface casing shoe. It was determined that, due to the shallow interventions in close proximity to each other, with no porous formations between them, there was no incremental risk to isolating the shallower source before waiting for confirmation of success from the first (deeper) intervention.

The intervention on WEE-2 was completed on 20–21 November 2019. The first set of dents (bottom of the Shaftsbury Fm.) was applied using the EE-MS tool. After the first set, the tool string was run down past the dents, to confirm whether the dents were placed successfully by observing the casing collar locator. However, the tool string could not be run in hole past a point 1.4 m below the lowest dent. Investigation showed this was due to debris from the Energetic Expander tool, including a solid steel extension, specific for the EE-MS design. The blockage was resolved using a magnet. Because of this observation, the upper set of dents was placed using the EE-SS tool. Based on these learnings, the EE-MS tool design was later modified.

The vent flow rate before the intervention fluctuated significantly, with an average over the eight days immediately leading up to the intervention of 90 L/day (Fig. 16c). Similar to WEE-1, the increased time between the placement of consecutive sets of dents, needed to change out tools, made it possible to identify the flow-reduction impact of each dented interval (Fig. 16d). Based hereon, it appears that the set of dents deployed using the EE-MS in the base of the Shaftsbury Fm. initiated the downward trend in flow rate. It is not clear whether the three dents inside the surface casing had an additional effect on the flow rate decline, as the large fluctuations may mask smaller changes. Notably, when pressure was applied to the casing during a 10-min 7 MPa pressure test and subsequent CBL pressure pass, it was clear that the ballooning effect on the casing caused a flow restriction, followed by a flow surge when pressure was bled off. The flow rate continued to decline over a period of 50 days, at which point the flow registered zero. From 11 to 20 January 2020, the monitoring system recorded no flow, likely attributable to colder ambient temperatures during that period. Flow was measured again on 21 January and the bleed-off trend resumed. For the last ten days of recording, flow rate averaged 11 L/day with fluctuations that generally appeared to correlate with daily temperature fluctuations. When the vent flow monitoring device was removed on 22 February 2020 a 10-min regulatory bubble test was performed, with zero bubbles observed. Due to the fluctuating nature of the flow, this result will not be considered conclusive.

7.2.3. Energetic expander well 3 (WEE-3): November 2019

WEE-3 is a vertical legacy well located in the southern Sundown area of the field, drilled and completed in the Doig Fm. in 2004. It has 244.5 mm surface casing, landed at 499 mKB and cemented successfully with returns to surface, and 177.8 mm 38.68 kg/m L80 intermediate casing, landed at 3105 mKB. A 114.3 mm production liner was also installed, with the liner top at 2946 mKB (i.e. below the area of interest for this SCVF remediation). Unlike the other test wells, the intermediate casing did not have cement returns to surface. Upon completion in 2004, a pre-frac bubble test was performed with zero flow recorded. WEE-3 produced from the Doig Fm. with a packer completion until 2011. Zonal abandonment of the Doig Fm. was completed in 2016. Prior to abandonment, a 10-min bubble test again indicated no SCVF. During the abandonment operation, flow (including methane gas and drilling mud) was observed from the surface casing vent when 3.5 MPa pressure was applied to the casing. Diagnostic work concluded the casing was breached between ~700 and 900 mKB, with communication from the breach to surface through the vent assembly. Top of annular cement was observed on a radial CBL at 1220 mKB. The breach and other potential casing corrosion issues across the uncemented interval were remediated by pumping 1900 kg/m^3 Portland Class G cement using a retainer. Circulation was achieved with good cement returns and the top of cement inside casing was left at 675 mKB. A post-cementing bubble test indicated no flow. A follow-up bubble-test the next summer failed, indicating the well had developed SCVF after the remedial cement job. This type of failure has been observed frequently in remedial cementing operations, and is likely due to the lack of a proper annular cement base, allowing the cement to slump, or poor mud removal. In two years of monitoring, the highest flow rate recorded was 1351 L/day, and the highest stabilised build-up pressure was 2922 kPa.

A radial CBL of the remedial cement job was collected in 2019, in preparation for SCVF remediation. Geochemical analysis indicated shallow gas, but was unable to relate it to a specific formation. The only shallow formation in the wellbore with both porosity and possible gas signature from log analysis was the Dunvegan Fm. This information, in combination with the CBL analysis and the well history, resulted in a qualitative decision to place the first set of dents in the shallower Kaskapau Shale, at a depth with the best combination of competent non-porous rock and high cement bond index in CBL logs. A second set of dents was planned just inside the surface casing shoe, for final isolation and as a mitigation against the uncertainty associated with the inconclusive geochemical analysis. In addition to the two sets of dents for isolation, two extra intervals were selected to evaluate the ability of the Energetic Expander tool to achieve an improvement in the bond index of initially bad quality cement, and thereby begin to establish the operational boundary conditions for the tool. A set was planned at 625 mKB, where both pressure and non-pressure pass indicated a bond index of ~0.5 (poor bond, no micro-annulus), and at 575 mKB where 0 MPa pass indicated bond index of about 0.6, and pressure pass indicated a slight improvement to about 0.75 (poor bond, micro-annulus). Because all selected dent depths were shallow, in close proximity, and normally pressured with no additional porous intervals between them, there was no perceived incremental risk to completing all interventions in one visit without additional monitoring and verification in between.

The trial on WEE-3 was completed on 22–23 November 2019. Three dents were placed for Interval 1 (645.5–646.5 mKB, in Kaskapau Fm., for the Dunvegan source) between 12:30 h and 17:45 h on 22 November. The following day, between 09:00 h and 11:00 h, three dents were placed for Interval 2 (489–491.5 mKB, inside surface casing, for final isolation). The three dents for Interval 3 (574.5–575.8 mKB, Cardium Fm., extra dents for research) were placed between 12:30 h and 14:30 h. For Interval 4 (624.5–625.5 mKB, Kaskapau Fm., extra dents for research), two dents were placed between 15:15 h and 16:30 h on 23 November 2019. The third dent was not placed for this last interval, due to an earlier misrun.

Because the vent flow monitoring device could be installed only 27 h before the first dent was placed, it is not possible to establish a trend in the initial flow data (Fig. 16e). The average flow rate for this time period was 1310 L/day. Data was not collected between 22 November, 11:38 h, and 23 November, 16:48 h, due to an operator error. As such it is not possible to determine the sealing contributions from individual dent intervals. When the vent flow monitoring device was turned on after the final dent, the flow rate had started to decline rapidly. On 24 November, 10:30 h, flow rate had reduced to 670 L/day. Subsequently, a casing calliper log and CBL were performed across the dented intervals. While preparing to perform the CBL pressure pass, a 7 MPa pressure test failed with rapid bleed off, indicating a casing breach had occurred. These logging results and observations will be discussed further below. The pressure test is visible in the flow rate data as a small fluctuation (Fig. 16e), but clearly did not interrupt the overall decline. Flow rate continued to decrease exponentially, effectively reaching zero on 4 December 2019, eleven days after the intervention was completed. The monitoring device remained installed for eight days, during which

no flow was measured. After it was removed on 12 December 2019, a regulatory bubble test was performed, also indicating zero flow.

7.3. Cement bond log (CBL) and calliper data

For comparison, "pre-dent" cement bond log (CBL) data, obtained sometime prior to the field trials, were available for all six test wells (Table 3). These data included CBLs obtained while the well was pressurised (7 MPa) and non-pressurised (0 MPa). To maximise the learnings from the field trials, post-intervention CBLs and calliper logs were obtained for the dented intervals of wells WEE-2 and WEE-3. In the following, we first present and compare the pre- and post-dent CBL and post-dent internal casing calliper data for these two wells, after which the pre-dent CBL data of all trial wells will be analyzed in an attempt to delineate tool efficiency in SCVF remediation. Although the interpretation of bond indices from CBLs in post-dent analyses suffers from the expanded and deformed casing shape, this uncertainty is not thought to greatly impact the interpretation of the improved bond index due to densified cement in the casing-formation annulus. Previous works and studies quantifying the change in bond tool amplitude responses suggest such effects could be present (Anderson and Walker, 1961; Fulton, 1979; Pardue and Morris, 1963), but it is expected that the uncertainty introduced into evaluating bond indices for WEE-2 and WEE-3 is minor.

7.3.1. WEE-2 pre- and post-dent CBL comparison

Fig. 17 shows the "pre-dent" CBL of the dent interval located inside the surface casing (Interval 2, 393–396 m), obtained prior to the field trial, plotted together with the "post-dent" CBL, 40-arm calliper and temperature logs that were recorded ~12 h after denting. The bond index improvement post-denting is evident under both non-pressure and pressure logging conditions for this upper dent interval. Inside the surface casing, the three dents were created separately, in order bottom-top-middle, with tool centralization performed independently for each dent placed. Calliper measurements (Fig. 17b) show localized and radially uniform casing deformation (13–20% ID increase), suggesting good tool centralization. Similarly, the pre- and post-dent CBL of the lower dented interval in the Shaftsbury Shale Fm. (Interval 1, 480–481 m) show an improved bond index at both 0 and 7 MPa pressure (Fig. 18a). Note these dents were created using the EE-MS tool, with effective centralization only occurring above the tool assembly. While the casing deformation is still well localized, the non-uniform deformation suggests poorer centralization of the middle and bottom explosive charges. The increase in casing ID ranges 13–18%, 13–26%, and 13–31% for the top, middle, and bottom dents respectively (Fig. 18b). These calliper data demonstrated tool centralization is negatively impacted further away from the tool string centralizer when deploying a 18.9 kg EE-MS assembly, whereas a single shot only weights 4.9 kg.

7.3.2. WEE-3 pre- and post-dent CBL comparison

Figs. 19–22 show pre- and post-dent CBL, 40-arm calliper, and temperature logs that were recorded ~20 h after denting with the energetic expander for the four dented intervals along WEE-3. Note these intervals include (Section 7.2.3):

- Interval 1: 645.5–646.5 mKB, in the Kaskapau Fm., for the Dunvegan source
- Interval 2: 489.0–491.5 mKB, inside the surface casing for final isolation
- Interval 3: 574.5–575.8 mKB, in the Cardium Fm. (extra dents for research purposes)
- Interval 4: 624.5–625.5 mKB, in the Kaskapau Fm. (extra dents for research purposes)

Due to a breach in the casing, a post-dent pressure pass CBL was not

Table 3
Overview of field trial data. B = bottom, M = middle, T = top. *dents created simultaneously using EE-MS tool, **post-intervention vent flow occurred in progressively infrequent pulses. DVGN denotes Dunvegan well, Alberta Canada.

well ID	interval #	depth	dent sequence	dent spacing	pre-dent CBL bond index		post-dent CBL bond index	
					0 MPa	7 MPa	0 MPa	7 MPa
		[mKB]		[cm]	[-]	[-]	[-]	[-]
WLE-1	1	508–509	B-T-M	~30	0.16	0.76		
	2	569–570	B-T-M	~30	0.23	0.82		
	3	606–607	B-T-M	~30	0.35	0.88		
	4	371–372	B-T-M	~30	0.04	0.49		
	5	364–365.5	B-T-M	~30	0.04	0.46		
WLE-2	1	1048–1049	B-T-M	~30	0.10	0.42		
	2	1045–1046	B-T-M	~30	0.06	0.34		
	3	1040–1041	B-T-M	~30	0.09	0.37		
	4	1034–1035	B-T-M	~30	0.13	0.38		
	5	838–839	B-T-M	~30	0.84	0.94		
	6	623–624	B-T-M	~30	0.32	0.98		
	7	200–201	B-T-M	~30	0.07	1.00		
	8	190–191	B-T-M	~30	0.14	0.55		
WLE-3	1	1272–1273	B-T-M	~30	0.90	1.00		
	2	1265–1266	B-T-M	~30	0.88	1.00		
	3	552–553	B-T-M	~30	0.65	0.94		
	4	540–541	B-T-M	~30	0.72	1.00		
	5	456–457	B-T-M	~30	0.50	1.00		
	6	445–446	B-T-M	~30	0.47	1.00		
WEE-1	1	1244–1245	B-T-M	~50	0.77	0.92		
	2	797–798	B-T-M	~50	0.94	0.99		
	3	432–433	B-T-M	~50	0.10	0.63		
WEE-2	1*	480–481	3 × 1 MS	~30	0.05	1.00	0.68	1.00
	2	395–396	B-T-M	~50	0.27	1.00	0.84	1.00
WEE-3	1	645–647	B-T-M	~50	0.96	1.00	1.00	
	2	491–492	B-T-M	~50	0.97	1.00	1.00	
	3	575–576	M-T-B	~50	0.28	0.40	0.43	
	4	625–626	B-T	~50	0.20	0.40	0.20	
DVGN	1	535–538		~100	1.00	1.00	1.00	1.00
	2	359–363		~100	0.60	0.90	1.00	1.00

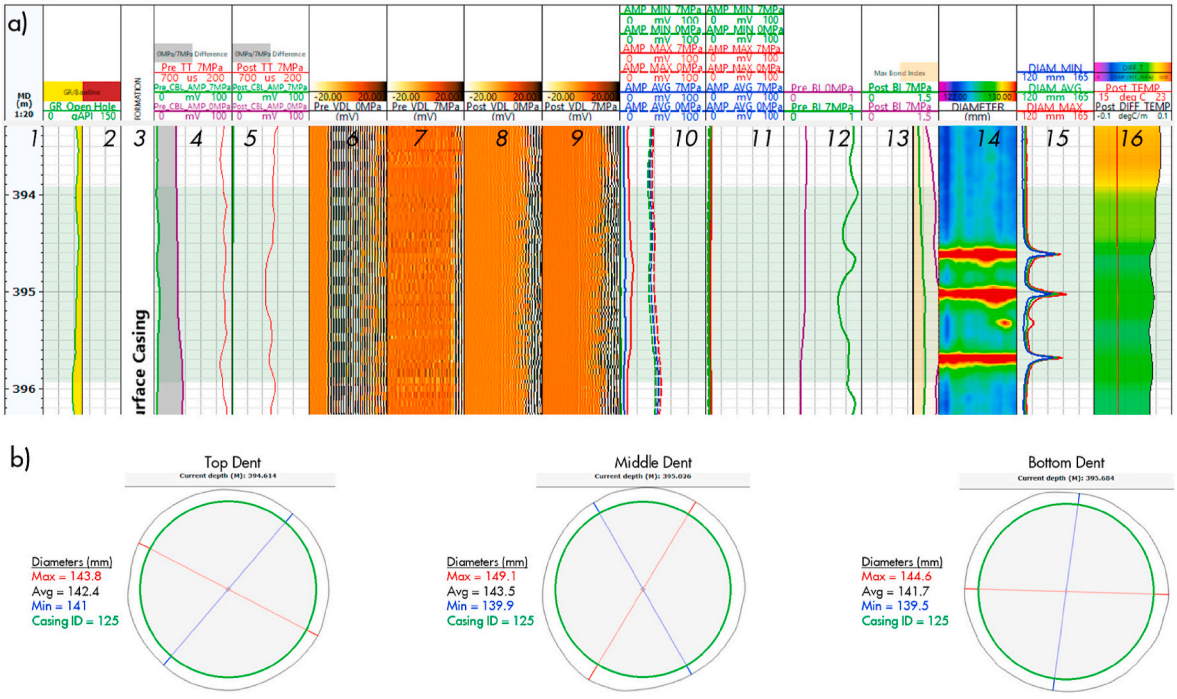

Fig. 17. WEE-2 Interval 2, with a) Log panel layout of pre- and post-dent CBL and post-dent calliper logs. Track description from left to right: 1: Measured depth from Kelly Bushing [m], 2: Gamma ray measurement from open hole logs, 3: Interval and formation identifier, 4/5: Pre-dent and post-dent CBL measurements respectively. Red – 7 MPa pressure pass travel time (TT), green – 7 MPa CBL amplitude, purple – 0 MPa CBL amplitude, grey fill – difference between 0 MPa and 7 MPa indicating microannuli, 6/7: Pre-dent variable density log (VDL) at 0 MP and 7 MPa respectively, 8/9: Post-dent variable density log (VDL) at 0 MP and 7 MPa respectively, 10/11: pre- and post-dent radial bond measurements of minimum, average, and maximum amplitudes at 0 MPa and 7 MPa, 12/13: pre- and post-dent bond index interpretations, green- 7 MPa bond index, purple – 0 MPa bond index interpretation, yellow fill – bond index above theoretical maximum of 1, 14: Colour map of 40-finger internal casing calliper log, 15: Maximum, average, and minimum internal diameters from 40-finger calliper log, 16: Post-dent temperature measurements, red line – absolute temperature, colour fill – differential temperature in depth; b) cross-section representations of casing shape post-dent for each dent in dent interval. (For interpretation of the references to colour in this figure legend, the reader is referred to the Web version of this article.)

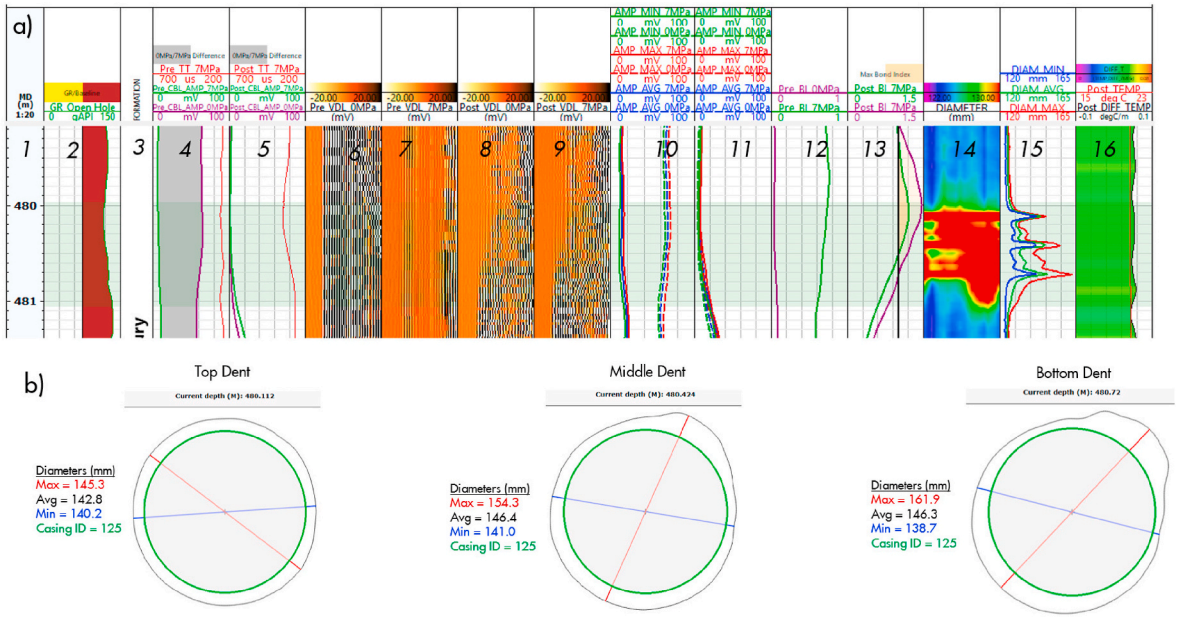

Fig. 18. WEE-2 Interval 1, with a) Log panel layout of pre- and post-dent cement bond long and post-dent calliper logs. Track layout identical to Fig. 17 b) cross-section representations of casing shape post-dent for each dent in dent interval.

achievable. All intervals showed an improved bond index on the 0 MPa post-dent CBL. Based on post-dent calliper logs, eccentric and irregular casing deformation occurred (Figs. 19b–22b). Possible casing breaches and splits (Fig. 23) were observed across multiple dented areas. Currently, this casing breach is thought to be a result of poor tool centralization and poor casing integrity, due to the late life remedial cement job, in combination with too large a charge load (258 g) for controlled expansion in this casing type in this particular condition. In

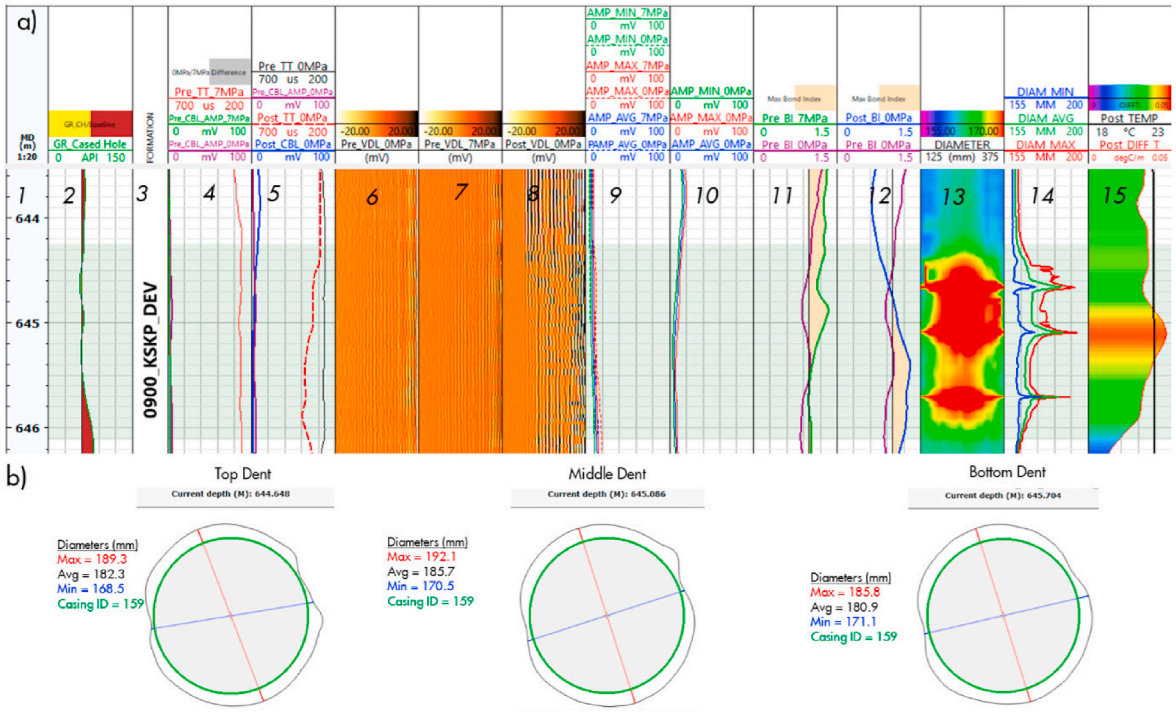

Fig. 19. WEE-3 Interval 1, with a) Log panel layout of pre- and post-dent CBL and post-dent caliper logs. Track description from left to right: 1: Measured depth from Kelly Bushing [m], 2: Gamma ray measurement from cased hole logs, 3: Interval and formation identifier, 4: Pre-dent and post-dent CBL respectively. Red – 7 MPa pressure pass travel time (TT), green – 7 MPa CBL amplitude, purple – 0 MPa CBL amplitude, grey fill – difference between 0 MPa and 7 MPa indicating microannuli, 5: Pre and post-dent CBL 0 MPa measurements. Red dash – post-dent 0 MPa TT, black – pre-dent 0 MPa TT, purple – pre-dent 0 MPa CBL amplitude, blue – post-dent 0 MPa CBL amplitude, 6/7: Pre-dent variable density log (VDL) at 0 MPa and 7 MPa respectively, 8: Post-dent variable density log (VDL) at 0 MPa, 9/10: Pre- and post-dent radial bond measurements respectively of minimum, average, and maximum amplitudes at 0 MPa and 7 MPa, where available, 11/12: pre- and post-dent bond index interpretations, green-pre-dent 7 MPa bond index, purple – pre-dent 0 MPa bond index interpretation, blue – post-dent 0 MPa bond index, yellow fill – bond index above theoretical maximum of 1, 13: Colour map of 40-finger internal casing caliper log, 14: Maximum, average, and minimum ID from 40-finger caliper log, 16: Post-dent temperature measurements, absolute temperature (red line) and differential temperature in depth (colour fill); b) cross-section representations of casing shape post-dent for each dent in the dented interval. (For interpretation of the references to colour in this figure legend, the reader is referred to the Web version of this article.)

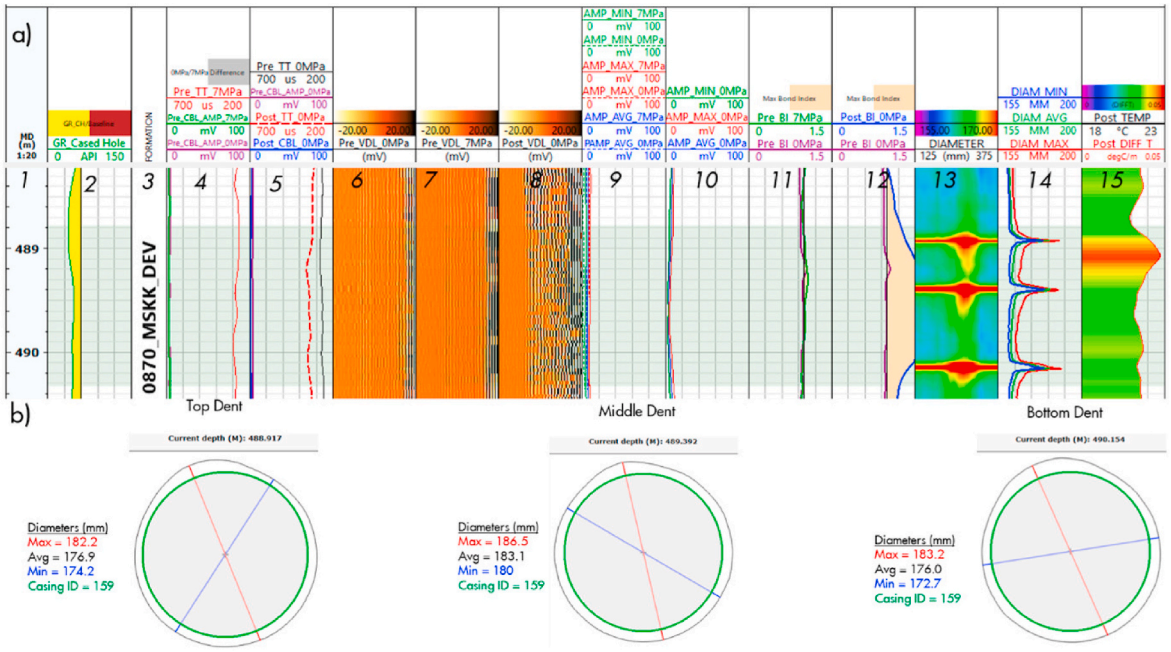

Fig. 20. WEE-3 Interval 2, with a) Log panel layout of pre- and post-dent cement bond long and post-dent caliper logs. Track layout identical to Fig. 19; b) Cross section representations of casing shape post-dent for each dent in dent interval.

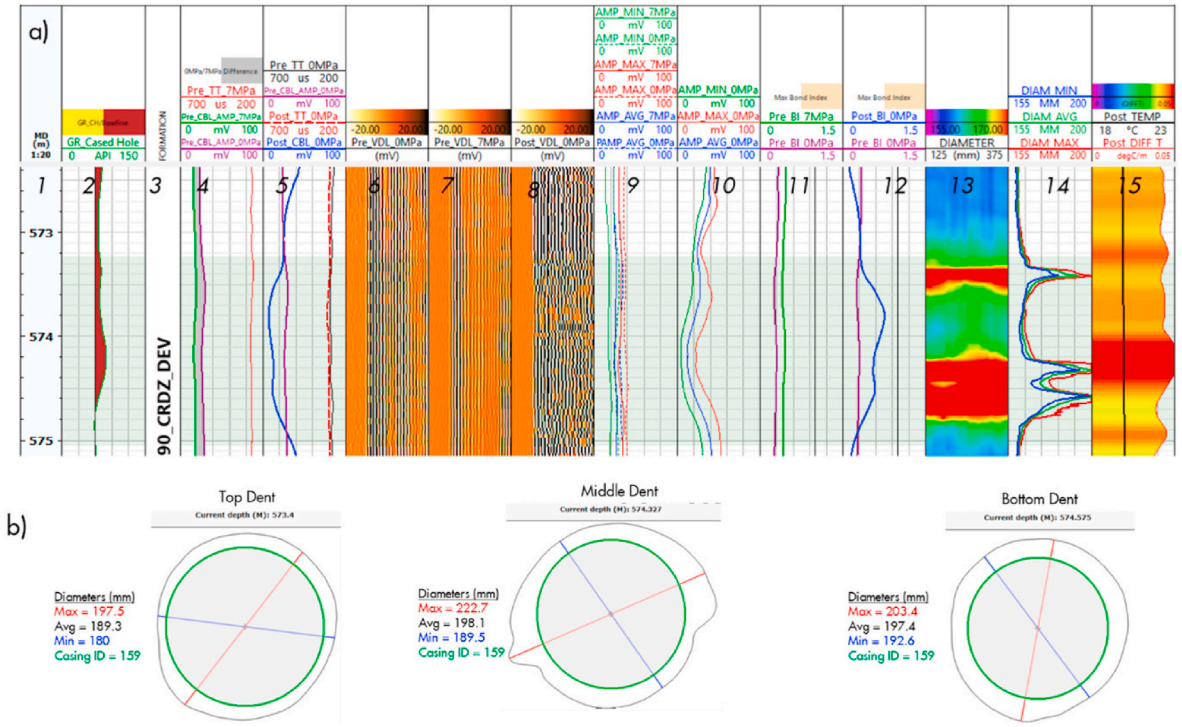

Fig. 21. WEE-3 Interval 3, with a) Log panel layout of pre- and post-dent cement bond long and post-dent caliper logs. Track layout identical to Fig. 19; b) Cross section representations of casing shape post-dent for each dent in dent interval.

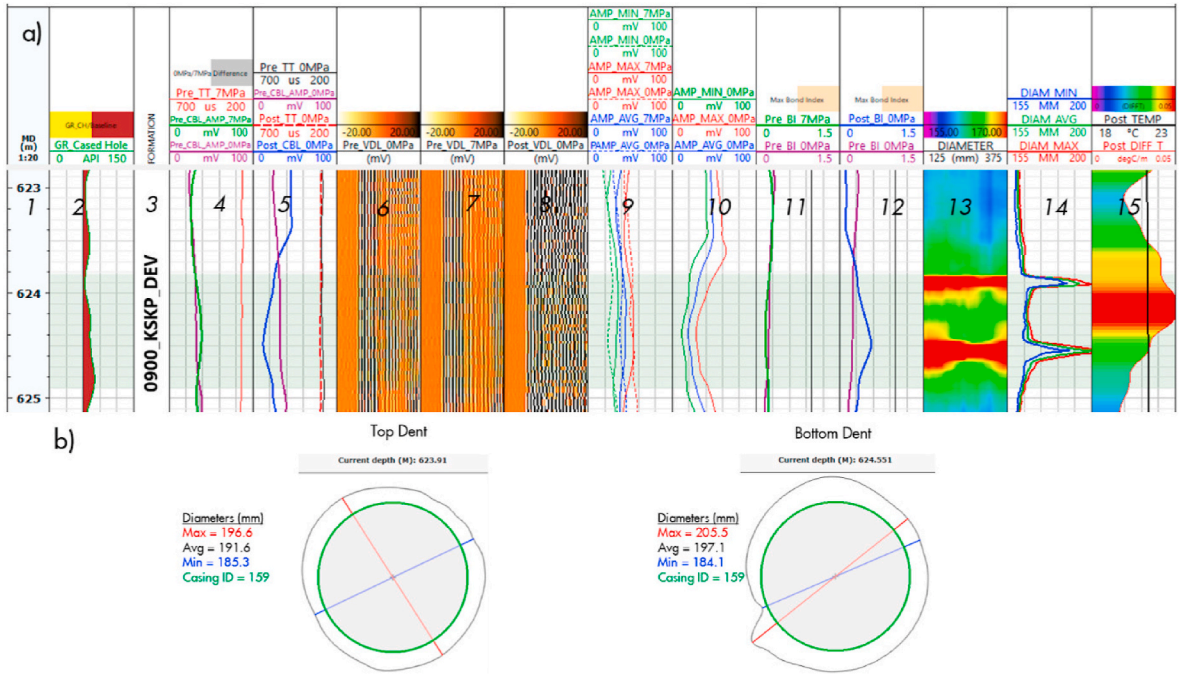

Fig. 22. WEE-3 Interval 4, with a) Log panel layout of pre- and post-dent cement bond long and post-dent caliper logs. Track layout identical to Fig. 19; b) Cross section representations of casing shape post-dent for each dent in dent interval.

this respect, it should be noted that the 40-arm calliper run also showed a casing breach at 577.7 m, i.e. about 2 m below the dents of Interval 3, demonstrating that casing integrity was poor and a casing breach/irregular expansions were probably unavoidable.

7.3.3. *Pre-dent CBL data analysis for all test wells*

Fig. 24 shows the pre- and post-intervention bond indices available for WEE-2 and WEE-3, as well as data for a recent field trial of the Energetic Expander tool in Alberta, Canada (well denoted DVGN, further mentioned in Section 8.1). The data illustrate the range of pre-intervention bond index conditions that were improved using LCE technologies. As detailed in Section 7.2.2, WEE-2, Interval 2 was identified as being the dent successful in reducing SCVF. It can therefore be inferred that the pre-dent bond conditions at WEE-2, Interval 2, were

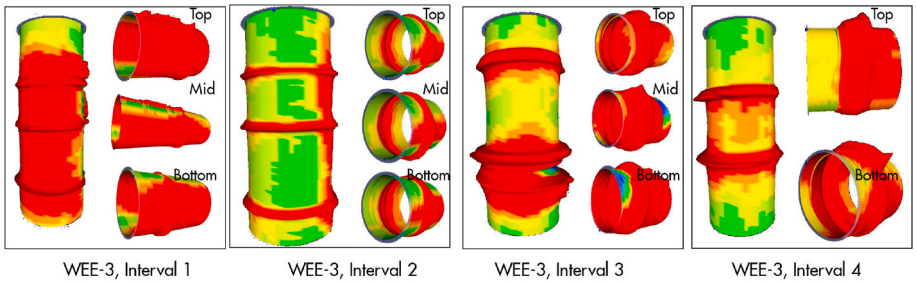

Fig. 23. Expander intervals in WEE-3 casing deformations from 40-arm calliper data, showing individual dents as well as non-uniform deformation and potential casing breaches. Reddish colours indicate enlarged radii, Green colours represent nominal ID values, while blue colours indicate smaller radii. (For interpretation of the references to colour in this figure legend, the reader is referred to the Web version of this article.)

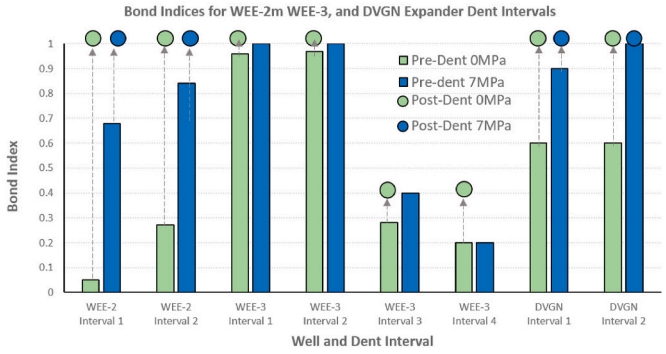

Fig. 24. Pre- and post-intervention bond indices for all LCE intervals in WEE-2, WEE-3, and DVGN. Bars and dots illustrate pre- and post-intervention bond index evaluations respectively. Data obtained under non-pressurised conditions, denoted 0 MPa, are shown in green, data obtained while the well was pressurised to 7 MPa are shown in blue. (For interpretation of the references to colour in this figure legend, the reader is referred to the Web version of this article.)

improved during the LCE process in such a way as to provide hydraulic isolation. Indeed, the interval is characterised by greatly improved bond indices and a reduced micro-annulus in the post-dent bond analysis. From this observation, it may be further inferred that pre-dent bond conditions of the same quality or better (i.e. smaller micro-annuli, better pressurised/non-pressurised bond index) could be improved using LCE technologies to provide hydraulic isolation.

The bond indices available from pre-dent, non-pressurised (0 MPa) and pressurised (7 MPa) CBLs for the dented intervals of all trial wells are plotted in Fig. 25. Following the reasoning above, dents WEE-2, Interval 2, WEE-3, Interval 1, WEE-3, Interval 2, DVGN, Interval 1 and DVGN, Interval 2 (see Table 3) define Polygon 1 (green, Fig. 25), a region of pre-dent bond index conditions over which the expander tools were capable of successfully achieving hydraulic isolation with a quantifiable and similar bond index improvements. Fig. 25, Polygon 2 (light yellow), highlights the case study intervals with pre-dent bond conditions similar to or better than those in Polygon 1, suggesting that hydraulic isolation via expanders is achievable in this region of pre-dent bond indices. Lastly, Fig. 25, Polygon 3 (indicated in grey), illustrates the region of pre-dent bond conditions over which it is unverified and/or untested if hydraulic isolation via LCE can be achieved. It is possible that conditions of pre-dent bond quality in Polygon 3 are suitable to provide hydraulic isolation after denting, but these conditions could not be identified in the available field data. Going forward, this analysis may be used to justify hydraulic isolation interventions via LCE operations and opportunities to expand the tested range will be considered.

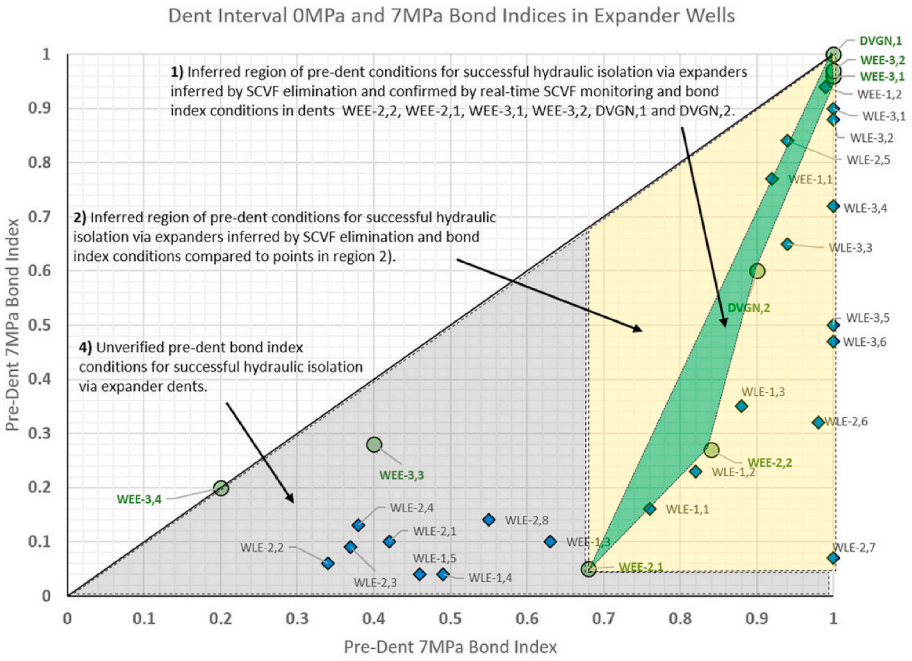

Fig. 25. Range of pre-intervention bond indices for all dent intervals across six field trial wells, i.e. including both Local Expander and Energetic Expander tool data, with interpreted ranges of successful, inferred, and unverified conditions for hydraulic isolation for given pre-dent cement bond quality. Green circles are wells with post-dent logging, blue diamonds for wells without post-dent logging. See main text for discussion. (For interpretation of the references to colour in this figure legend, the reader is referred to the Web version of this article.)

8. Discussion

8.1. Effectiveness of LCE technologies in SCP/SCVF remediation

The LCE-concept in general, and the Local Expander and Energetic Expander tools in particular, have been extensively tested in both lab experiments and field trials. In the laboratory studies, use of the LCE tools to create dents in the innermost casing pipe of full-scale, cemented wellbore samples (which initially contained microannuli and other defects) is found to invariably improve sealing performance (Section 6.1). In the majority of cases, LCE even resulted in effective restoration of zonal isolation along the length of the lab samples, as evidenced by the low post-dent equivalent permeability of the cemented annuli (Figs. 6d and 7d), which attained values rivalling the sealing performance that could theoretically be expected from a full-length section of perfectly-bonded, defect-free cement (which has matrix permeabilities in the range of 10^{-21} to 10^{-17} $m^2 = 1$ nD to 10 μD (Montgomery, 2006; Taylor, 1992)). These findings corroborate those of Kupresan et al. (2014, 2013), who previously observed noteworthy reductions in the permeability of lab-scale cemented annuli upon expansion of the samples' inner steel tube using a conical expansion mandrel. In the present study, this beneficial effect of LCE on annular sealing performance could in principle be extended to dual annulus configurations, where use of a Local Expander tool achieved a hundredfold decrease in seepage rate along the second cemented annulus of a dual annulus lab sample (Fig. 6c, Section 6.1.1). However, additional research is required to better understand how complete zonal isolation can be reliably achieved in such multi-annulus configurations. Whether LCE technologies can also effectively close and remediate larger defects, such as mud channels, is still subject of ongoing laboratory research, but preliminary results are rather promising.

Turning to the field trials, implementation of both the Local Expander and Energetic Expander tools was generally successful (Section 7). All six Groundbirch trial wells are currently classified as "suspended" and remain part of an annual field-wide SCVF monitoring programme. Per Shell Groundbirch internal best practice, each well has to undergo a minimum of one annual monitoring cycle prior to concluding that the SCVF has been permanently eliminated. Results for the summer SCVF testing campaign of 2019 indicated zero residual flow on WLE-1 and WLE-2, corroborating the short-term observations (Fig. 15a–b), while the other four wells (WLE-3, WEE-1, WEE-2 and WEE-3) were still pre- or mid-intervention at the time. All six trial wells were included in the Summer 2020 SCVF testing campaign, with each indicating zero residual flow. Next steps include completion of the abandonment of all test wells with 100% SCVF elimination per the above criteria, by placing plug and cement isolations inside casing at selected caprock intervals in order to achieve formation-to-formation isolations, as well as mitigate against future casing failure at dented intervals, prior to commencing surface (cut, cap and reclamation) activities. Additionally, Shell Canada is pursuing rapid replication of these successful field trials with campaign-style abandonment work for 2020. As SCVF wells of increasing complexity (including additional casing sizes, weights and grades; cement quality threshold reductions and casing integrity challenges) are addressed with expanders, the applicability range for these tools will become further defined.

The success of the Canadian field trials also drove wider replication efforts in early 2020. In February 2020, five wells in Shell's Appalachia asset (United States) were remediated using an Energetic Expander tool, with a 50 cm dent spacing. While the CBL results for these trials are inconclusive, vent flow measurements show remediation was effective, eliminating about 2110 L/day of methane-equivalent emissions from SCVF. In April 2020, an Energetic Expander tool was successfully deployed using a 100 cm dent spacing in Alberta, Canada. CBL results for this well are appended to Table 3. Calliper log results showed expansion ratios in line with predictions and established uniform pipe deformation was achieved. Casing integrity was retained and confirmed by a 7 MPa pressure test. Annular vent flow monitoring is still ongoing, but showed a 92% reduction in SCVF and 98% reduction in SCP within the first two weeks. Additional interventions, using 4-1/2″ and 7″ models of the Local Expander tool and the EE-MS tool, are in various stages of planning and execution.

8.2. Impact of LCE on cement structure and properties

LCE technologies impose large stresses and strains on the casing pipe to locally enlarge its diameter. The associated deformations affect not only the casing itself, but also impact the adjacent cement sheath, additional casings and cement sheaths, plus surrounding rock formations. The intensity of deformation is expected to decrease quickly with distance from the innermost casing, however, as progressively larger volumes of interstitial material can redistribute and accommodate the displacements imposed at the central casing pipe. This is also evident from our laboratory tests, where relatively compliant behaviour of the annular cement limited and smoothed the deflection of the outer casing pipe (cf. casing on bottom of Fig. 8g). This pronounced deformation in the cement sheath is noteworthy, considering that rather large strains were accommodated without visible fracture or major loss of cohesion (Fig. 8). From a sealing perspective, at least, the laboratory experiments corroborate the cement structural integrity was retained, or even improved (Figs. 6 and 7).

To understand why the LCE-induced deformations could be sustained without significant cracking of the cement, it is important to appreciate the significant impact of confinement on the mechanical behaviour of cements. In conventional triaxial compressive tests, cement is known to become markedly more ductile under elevated confining pressure (Bažant et al., 1986; Li et al., 2019; Wolterbeek et al., 2016) as higher effective mean stresses generally promote compaction processes while inhibiting dilatational modes of failure (e.g. Jaeger et al., 2007). In the LCE experiments, this confinement is provided by the outer casing pipe, which prevents the cement sheath from spalling. This second casing restricts outward movement, forcing the annular volume reduction caused by indentation to be accommodated mostly internally, i.e. through closure of defects such as micro-annuli, fractures and other voids, resulting in an overall densification of the cement microstructure. In the LCE field trials, restraints are provided by the casing elements, as well as the lithostatic pressure and stiffness response of the surrounding rock formations. The profound impact of high confinement on cement deformation has been demonstrated in so-called "tube squash tests" (Bažant et al., 1999; Caner and Bažant, 2002), where cylindrical samples of cement and concrete can be shortened to large strains, under high confinement provided by ductile steel alloy tubes. Remarkably, cement samples thus deformed were able to sustain about 50% axial shortening strain without developing any visually detectable cracks, instead showing high-angle (over 70°) cohesive shear bands (Bažant et al., 1999), not unlike to the ones observed in our LCE experiments (Fig. 8g). Bažant et al. (1999) further performed uniaxial compression and Brazilian split cylinder tests on smaller cores drilled from their deformed samples. They found that the compressive strength of the deformed cement paste cores was about 30% of the corresponding virgin cement paste compressive strength, while the tensile strength of the deformed cement paste was about 50–60% of its initial tensile strength (see Table 4 of Bažant et al., 1999). Similar weakening may occur in close proximity to the LCE dents, where the strains are largest, but is considered unlikely further away from the dents. Accordingly, the locally dented zones can be supported and constrained by the remainder of the cement column, which will continue to provide mechanical and frictional strength. Song et al. (2001) studied the microstructure of the cement samples deformed by Bažant et al. (1999), concluding that the movement and redistribution of hydrated phases contributed to the increased ductility. Essentially similar results were obtained in the present study and by Kupresan et al. (2014, 2013), who reported the cement in their tests deformed by a combination of pore collapse, matrix densification

and displacement of free pore water.

Further research is being performed to increase understanding of the operable range of LCE technologies, e.g. in terms of the minimum degree of confinement required to ensure stable mechanical behaviour of the cement sheath. While this may impose limitations on LCE technology use on cement sheaths directly against weak or shallow formations, it should be noted that we have observed no such issues in any of the field trials performed to date (e.g. none of the test wells developed signs of gas migration after the LCE-tool interventions). This could be related to the fact that shallower rock formations are generally shielded by multiple casing annuli, with the LCE-induced deformations being largely dampened within the first few cemented annuli (cf. Fig. 8g), rather than directly impacting the rock formations. Further consideration should nevertheless be given to determining the proper amount and application rate of LCE for a given wellbore configuration. Especially with the Local Expander tool (which creates the indentations in a mechanical, very controlled manner) these properties can principally be tailored for purpose as needed.

8.3. Impact on casing strength and implications for well design and operations

The current casing integrity studies have only considered burst and collapse loading. Hereby, it is implied that the pipe material has sufficient ductility to survive the denting process and any additional plastic set during the loading phases. Under this assumption, the performed calculations indicate that pipe denting locally enhances the collapse strength of a pipe (Fig. 12), while in practice the collapse strength will remain to be controlled by the pipe body. Therefore, no additional allowance needs to be considered for collapse design.

The finite element simulations further indicate that the residual stresses induced by the denting process (Fig. 11) do not have a significant effect on the ultimate internal pressure bearing capacity, as they are plastically relieved at relatively low pressure-levels (Fig. 13). Should the pipe be loaded further into the plastic regime, then through-wall plasticity and thinning initiate locally in the crestal-zone of the dent. However, these deformations can only grow large enough to become unstable if through-wall plasticity effects are also occurring in the adjacent pipe body material. The reduction in ultimate pressure bearing capacity caused by the dents is therefore small (Fig. 13).

In conventional well design, expected (pressure) loads should ideally be within the yield limits of the pipe (API TR 5C3, 2018), where additional design or safety factors may have been applied. Well loads within these design limits (of the undented pipe) may in the dented pipe cause some plastic relief of the residual stresses and some limited plastic set in the dent region, particularly in burst scenarios. However, only for cases of extreme unanticipated overloading (driving the confidence level of the design), the application of LCE causes catastrophic pipe failure to occur at slightly lower pressure (e.g. ultimate pressure bearing capacity of 778 versus 796 bar in dented versus undented pipe, Fig. 13). Such reduced ultimate strength levels will generally still be in excess of the structural or sealing limits of the pipe connections. In burst loading therefore, the connections may remain to drive the design. Furthermore, well tubular design generally considers the loads experienced during the entire functional life of the well, where the worst-case loading conditions driving the design generally occur during drilling or production phases. The loads experienced in the end-of-life abandonment phase will generally be more moderate and uncertainties in formation pressures, which may have affected the design phase, no longer exist. Additional allowance may be provided by the specific locations of the dents, which do not have to correspond to the critical well locations that drove the original design. Thus, in most practical applications, the small strength reductions predicted will only reduce the excess-strength at the location of the dents.

Note this study considered only the occurrence of plasticity and subsequent deformation mechanisms as would apply to the pipes made from materials having a minimum ductility to withstand the LCE process. Instable propagation of small pre-existing (but still undetectable during quality inspection) cracks, or environmentally assisted cracking could occur. These failure mechanisms have not been analyzed in detail and require further research.

8.4. Environmental and societal implications

In total, the three Local Expander tool and three Energetic Expander tool interventions, completed in Groundbirch, Canada between November 2018 and November 2019, have eliminated about 10,400 L/day of methane-equivalent emissions from SCVF (based on highest flow recorded in annual tests). In addition to the reduction in emissions attributable to the SCVF remedied, emissions associated with the intervention operation itself have been dramatically reduced as a result of the introduction of rigless SCVF remediation. An operation that previously required about five days of service rig operations, with various support equipment, including e-line, acid and cement trucks, can now be completed in one day with a small operational footprint, using only a masted e-line unit and a pressure truck. This accounts for a reduction in diesel consumption per SCVF intervention of over 90%. Additionally, the reduction in man-hours, trucking, and operational complexity results in a net reduction in Health, Safety and Environmental (HSE) exposure, and enables the industry to complete abandonment campaigns more efficiently, ultimately resulting in a greater impact to SCVF-related emissions reduction targets. In urban areas, the significantly smaller operational footprint would also allow interventions to be carried out with minimal disturbance.

8.5. Regulatory challenges

In many jurisdictions, current regulations have detailed requirements for annular hydraulic isolation which dictate that specific cementing methods must be used, with specific guidance for products, volumes and coverage dimensions. In order for regulators to enable innovative and efficient solutions, regulations should be updated, where applicable, to be more outcome-based. Alternate methods or barrier materials are accepted provided the SCVF problem is resolved without introducing additional hazards, and longevity can be demonstrated by theoretical modelling, laboratory and field test results.

In Alberta and British Columbia, Canada, the incumbent method of eliminating SCVF or achieving hydraulic isolation between porous zones is to perforate a 3–4 m interval at the top of the source formation, i.e. juxtaposed against a suitable caprock, and squeeze cement into the perforations (Energy Safety Canada, 2020). While regulations do not dictate perforation methods or the length of the cemented interval, the required outcome is clear as the well cannot be fully abandoned until no residual annular leakage remains. In order to support these outcome-based regulations, for the Canadian field trials of our LCE technologies, additional cement logging data has been collected and the bond improvement evaluated (Section 7.3). These results indicate that each set of casing expansions impacts the cement over substantially longer length than the affected casing length. Combined with the pre- and post-intervention vent flow measurements, these field results provide strong evidence to suggest that the efficacy of an annular seal is not solely dependent on length of the barrier, but more so on the quality of the barrier. This is corroborated by the laboratory testing, where single (sets of) dents achieved an improved seal against differential pressure comparable to the transport properties of much longer intervals of perfectly bonded cement (Section 6.1). As methods which offer higher efficiency of annular hydraulic isolation remediation are introduced and qualified, trial results can be used as supporting evidence to move away from prescriptive regulations and towards outcome-based regulations, enabling these more efficient methods.

9. Summary and conclusions

This study presents the results of an extensive research programme, including laboratory, numerical modelling and field trial components, demonstrating localized casing expansion (LCE) technologies offer promising possibilities for the restoration of annular zonal isolation along wellbores. The LCE concept involves imposing permanent deformation on the innermost casing pipe to locally enlarge its diameter. The reduction in annular volume associated with such indentation of the casing results in the mechanical closure of defects such as micro-annuli or fractures, and causes an overall densification of the cement matrix. Two principally different methods for achieving the required casing expansion have been investigated, where the Local Expander tool imposes deformations mechanically, while the Energetic Expander tool makes use of tailored-shaped explosive charges. Both tools were found to be highly successful in the remediation of annular fluid migration. The main conclusions of the research programme are summarised as follows:

- In the laboratory experiments, implementation of both LCE tools invariably improved annular sealing performance in full-scale, cemented-casing assemblies. In the majority of experiments, the process achieved effective restoration of zonal isolation along the entire length of the lab samples, thus successfully repairing a non-sealing cement sheath.
- Microstructural study of LCE-affected cement sheath samples obtained from the laboratory tests showed the process does not result in cracking of the cement. Instead, the imposed deformations are accommodated through densification of the cement matrix and formation of cohesive shear bands. Possible implications for mechanical integrity are discussed.
- Finite element modelling of the LCE process and subsequent loading of the dented casing pipe to burst or collapse failure demonstrated indentation does not significantly reduce the pipe's collapse strength, while the impact on burst strength is shown to become relevant only in cases of extreme unanticipated overloading. These findings are supported by laboratory testing.
- The laboratory findings, field trial results and logging data show that one or multiple short lengths (about 1 m) of densified cement are effective in sealing against annular fluid migration.
- The Local Expander and Energetic Expander tools have enabled rigless remediation of sustained casing vent flow (SCVF) along six trial wells in Groundbirch, Canada. Initial SCVF-rates of 100–6000 L/day were reduced by over 90% within days to weeks after LCE-based intervention. Follow-up monitoring over an extended period in the Summer of 2020 indicated zero residual flow in all six trial wells. This has eliminated about 10,400 L/day of methane-equivalent emissions from SCVF.

Credit author statement

T.K.T. Wolterbeek: Conceptualization, Methodology, Formal Analysis, Investigation, Validation, Writing – Original Draft, Writing – Review & Editing, Visualization. E.K. Cornelissen: Conceptualization, Methodology, Validation, Investigation, Visualization. S. Nolan: Conceptualization, Resources, Methodology, Investigation, Validation, Resources, Writing – Original Draft, Project Administration. F. Todea: Methodology, Formal Analysis, Validation, Investigation, Writing – Original Draft, Visualization. W. Stam: Methodology, Investigation, Validation, Writing – Original Draft, Project Administration. S.M. Roggeband: Conceptualization, Methodology, Software, Formal Analysis, Investigation, Writing – Original Draft, Writing – Review & Editing, Visualization. L. Dam: Resources, Project Administration. E.J. van Riet: Formal Analysis, Writing – Review & Editing. F. Ruckert: Conceptualization, Methodology, Investigation. W.J.G. Keultjes: Conceptualization, Writing – Review & Editing, Supervision.

Declaration of competing interest

The authors declare that they have no known competing financial interests or personal relationships that could have appeared to influence the work reported in this paper.

Acknowledgements

This research was funded by Shell Global Solutions International B.V. The authors would like to thank Gideon Langedijk and Sam van Moorsel for technical assistance in the laboratory. Coen van Schie is thanked for valuable contributions to Local Expander tool design. We like to thank two anonymous reviewers for their constructive feedback. The support and permission to publish by W.T. Bell International, Inc. is greatly acknowledged.

Appendix A. Table 1 in imperial units

Table 1
Overview of Local Expander tool specifications. OD denotes outer diameter; * 'OD head (collapsed)' corresponds to the minimum required casing inner diameter (ID) drift size, required for the tool to move freely up and down the bore.

Local Expander tool expander head type (= target casing OD)	4-1/2″-model				7″-model					9-5/8″-model		
	4-1/2″	4-1/2″T	5-1/2″	5-1/2″CT	7″	7″CT	7-5/8″CT	9-5/8″	9-5/8″CT	9-5/8″CT	10-3/4″CT	13-3/8″CT
OD body [inch]	3.54	3.54	3.54	3.54	5.63	5.63	5.63	5.63	5.63	8.15	8.15	8.15
OD head (collapsed)*[inch]	3.62	3.54	4.29	4.25	6.02	6.02	6.61	8.37	8.27	8.27	9.09	12.00
OD head (expanded) [inch]	4.51	4.61	5.49	5.70	6.98	7.36	7.95	9.33	9.61	12.05	12.87	15.78
max. radial increase [inch]	0.44	0.54	0.60	0.73	0.48	0.67	0.67	0.48	0.67	1.89	1.89	1.89
max. stroke length [inch]	6.97	6.97	6.97	6.97	5.51	5.51	5.51	5.51	5.51	16.73	16.73	16.73
max. axial force [kN]	853	853	1192	1192	1438	1438	1438	1438	1438	3155	3155	3155
tool length [ft]	22.97	22.97	27.89	27.89	13.12	13.12	13.12	13.12	13.12	15.42	15.42	15.42
tool weight [lbs]	~660	~660	~770	~770	~770	~770	~770	~770	~770	1650	1650	1650

Appendix B. Supplementary data

Supplementary data to this article can be found online at https://doi.org/10.1016/j.petrol.2020.108103.

References

Agbasimalo, N., Radonjic, M., 2014. Experimental study of the impact of drilling fluid contamination on the integrity of cement–formation interface. J. Energy Resour. Technol. 136, 42908.

Alberta Energy Regulator, 2003. Directive 020: Well Abandonment 1–47.

Anderson, W.L., Walker, T., 1961. Acoustic cement bond logging. In: SPWLA 2nd Annual Logging Symposium. Society of Petrophysicists and Well-Log Analysts.

API TR 5C3, 2018. Technical Report on Equations and Calculations for Casing, Tubing, and Line Pipe Used as Casing or Tubing; and Performance Properties Tables for Casing and Tubing, seventh ed.

Arjomand, E., Bennett, T., Nguyen, G.D., 2018. Evaluation of cement sheath integrity subject to enhanced pressure. J. Petrol. Sci. Eng. 170, 1–13.

Bachu, S., Watson, T., 2006. Possible indicators for CO2 leakage along wells. In: 8th International Conference on Greenhouse Gas Control Technologies, pp. 19–22.

Bailey, G., 2009. The evolution of expandable technology. J. Petrol. Technol. 61, 36–38.

Barclay, I., Pellenbarg, J., Tettero, F., Pfeiffer, J., 2001. The beginning of the end: a review of abandonment and decommissioning practices. Oilfield Rev. 28–41.

Bargawi, R.A., Zhou, S., Al-Umran, M.I., Aghnim, W.A., 2005. Expandable tubular successfully scab off severe casing leaks. In: SPE/IADC Middle East Drilling Technology Conference and Exhibition, 12-14 September, Dubai, United Arab Emirates. Society of Petroleum Engineers. https://doi.org/10.2118/97357-MS.

Bauer, S., Beyer, C., Dethlefsen, F., Dietrich, P., Duttmann, R., Ebert, M., Feeser, V., Görke, U., Köber, R., Kolditz, O., Rabbel, W., Schanz, T., Schäfer, D., Würdemann, H., Dahmke, A., 2013. Impacts of the use of the geological subsurface for energy storage: an investigation concept. Environ. Earth Sci. 70, 3935–3943. https://doi.org/10.1007/s12665-013-2883-0.

Bažant, Z.P., Bishop, F.C., Chang, T.-P., 1986. Confined compression tests of cement paste and concrete up to 300 ksi. ACI J 33, 553–560.

Bažant, Z.P., Kim, J.J.H., Brocca, M., 1999. Finite strain tube-squash test of concrete at high pressures and shear angles up to 70 degrees. ACI Mater. J. 96, 580–592.

BC Oil and Gas Commission, 2019. Oil & Gas Operations Manual, Appendix E: Technical Guidance for Determining the "Base of Useable Groundwater, pp. 189–190.

Bois, A.-P., Garnier, A., Galdiolo, G., Laudet, J.-B., 2010. Use of a mechanistic model to forecast cement-sheath integrity for CO2 storage. In: SPE International Conference on CO2 Capture, Storage, and Utilization. Society of Petroleum Engineers.

Bois, A.-P., Vu, M.-H., Noël, K., Badalamenti, A., Delabroy, L., Thérond, E., Hansen, K., 2018. Cement plug hydraulic integrity-the ultimate objective of cement plug integrity. In: SPE Norway One Day Seminar. Society of Petroleum Engineers.

Bosma, M., Ravi, K., Van Driel, W., Schreppers, G.J., 1999. Design approach to sealant selection for the life of the well. In: SPE Annual Technical Conference and Exhibition. Society of Petroleum Engineers.

Bosma, M.G.R., Cornelissen, E.K., Schwing, A., 2000. Improved experimental characterisation of cement/rubber zonal isolation materials. In: International Oil and Gas Conference and Exhibition in China. Society of Petroleum Engineers.

Boukhelifa, L., Moroni, N., James, S., Roy-Delage, L., Thiercelin, M.J., Lemaire, G., 2005. Evaluation of cement systems for oil and gas well zonal isolation in a full-scale annular geometry. SPE Drill. Complet. 20, 44–53.

Bourgoyne, A.T., Scott, S.L., Regg, J.B., 1999. Sustained casing pressure in offshore producing wells. In: Offshore Technology Conference. Offshore Technology Conference.

Brufatto, C., Cochran, J., Conn, L., Power, D., El-Zeghaty, S.Z.A.A., Fraboulet, B., Griffin, T., James, S., Munk, T., Justus, F., 2003. From mud to cement—building gas wells. Oilfield Rev. 15, 62–76.

Byrom, T.G., 2014. Casing and Liners for Drilling and Completion: Design and Application. Elsevier.

Campbell, K., Smith, R., 2013. Permanent well Abandonment. W. Ahead 9, 25–27.

Caner, F.C., Bažant, Z.P., 2002. Lateral confinement needed to suppress softening of concrete in compression. J. Eng. Mech. 128, 1304–1313.

Catto, N., 1991. Quaternary geology and landforms of the eastern Peace River region. In: British Columbia, NTS 94A/1, 2, 7, 8. Province of British Columbia, Ministry of Energy, Mines and Petroleum.

Chenevert, M.E., Shrestha, B.K., 1991. Chemical shrinkage properties of oilfield cements (includes associated paper 23477). SPE Drill. Eng. 6, 37–43.

Cornelissen, E.K., 2019. Method for Sealing Cavities in or Adjacent to a Cured Cement Sheath Surrounding a Well Casing. US 2019/0264547 A1.

Cowan, M., 2007. Field study results improve squeeze cementing success. In: Production and Operations Symposium, 31 March-3 April. U.S.A. Society of Petroleum Engineers, Oklahoma City, Oklahoma. https://doi.org/10.2118/106765-MS.

Davies, R.J., Almond, S., Ward, R.S., Jackson, R.B., Adams, C., Worrall, F., Herringshaw, L.G., Gluyas, J.G., Whitehead, M.A., 2014. Oil and gas wells and their integrity: implications for shale and unconventional resource exploitation. Mar. Petrol. Geol. 56, 239–254.

DeLange, R., Gandikota, R., Osburn, S., 2011. A major advancement in expandable connection performance, enabling reliable gastight expandable connections. SPE Drill. Complet. 26, 412–418.

Di Crescenzo, D., Shuster, M., Petlyuk, A., Ernens, D., Zijsling, D., Pasaribu, H., 2015. Lubricants and accelerated test methods for expandable tubular application. In: SPE/IADC Drilling Conference and Exhibition, 17-19 March. Society of Petroleum Engineers, London, England, UK. https://doi.org/10.2118/173111-MS.

Duncan, G., 2019. Methods for Preserving Zonal Isolation within a Subterranean Formation. US 10,480,294 B2.

Dusseault, M.B., Gray, M.N., Nawrocki, P. a, 2000. Why oilwells leak: cement behavior and long-term consequences. In: SPE International Oil and Gas Conference and Exhibition, SPE 64733, p. 8. https://doi.org/10.2118/64733-MS.

Energy Safety Canada, 2020. Wellbore Remediation; an Industry Recommended Practice (IRP) for the Canadian Oil and Gas Industry (Calgary).

Fanguy, C.J., Mueller, D.T., Doherty, D.R., 2004. Improved method of cementing solid expandable tubulars. In: SPE Annual Technical Conference and Exhibition. Society of Petroleum Engineers.

Filippov, A., Mack, R., Cook, L., York, P., Ring, L., McCoy, T., 1999. Expandable tubular solutions. In: SPE Annual Technical Conference and Exhibition. Society of Petroleum Engineers.

Fuller, G.A., Mercado, S., Mead, C., 2016. Engineered solutions to address deepwater remedial cementing challenges. In: IADC/SPE Drilling Conference and Exhibition. Society of Petroleum Engineers.

Fulton, D.K., 1979. Critical Factors Affecting Cement Bond Logs.

Gasda, S.E., Bachu, S., Celia, M.A., 2004. Spatial characterization of the location of potentially leaky wells penetrating a deep saline aquifer in a mature sedimentary basin. Environ. Geol. 46, 707–720. https://doi.org/10.1007/s00254-004-1073-5.

Goodwin, K.J., Crook, R.J., 1992. Cement sheath stress failure. SPE Drill. Eng. 7, 291–296.

Griffith, J.E., Lende, G., Ravi, K., Saasen, A., Nødland, N.E., Jordal, O.H., 2004. Foam cement engineering and implementation for cement sheath integrity at high temperature and high pressure. In: IADC/SPE Drilling Conference. Society of Petroleum Engineers.

Heathman, J.F., Beck, F.E., 2006. Finite element analysis couples casing and cement designs for HTHP wells in east Texas. In: IADC/SPE Drilling Conference. Society of Petroleum Engineers.

Hou, M.Z., Bauer, S., Kolditz, O., Xie, H., Li, X., Yang, C., Yuan, Y., 2013. Use of the geological subsurface for production, storage and conversion of clean energy. In: ISRM SINOROCK 2013, 18-20 June, Shanghai, China. International Society for Rock Mechanics.

Ingraffea, A.R., Wells, M.T., Santoro, R.L., Shonkoff, S.B.C., 2014. Assessment and risk analysis of casing and cement impairment in oil and gas wells in Pennsylvania, 2000–2012. Proc. Natl. Acad. Sci. 111, 10955–10960. https://doi.org/10.1073/pnas.1323422111.

ISO 10400:2018, 2018. Petroleum and Natural Gas Industries - Formulae and Calculations for the Properties of Casings, Tubing, Drill Pipe and Line Pipe Used as Casing or Tubing.

ISO 10426-2, 2005. Petroleum and Natural Gas Industries - Cements and Materials for Well Cementing - Part 2: Testing of Well Cements (ANSI/API Recommended Practice 10B-2).

Jaeger, J., Cook, N.G., Zimmerman, R.W., 2007. Fundamentals of Rock Mechanics, fourth ed. Blackwell Publishing.

Jandhyala, S.R.K., Pangu, G., Deshpande, A., Wolterbeek, T., Cornelissen, E., van Eijden, J., 2018. Volume change of cement plugs: spotlight on the role of boundary conditions using an improved testing method. In: SPE Asia Pacific Oil and Gas Conference and Exhibition. Society of Petroleum Engineers.

Joppe, L.C., Nelson, J.F., Kelman, G.L., 2017. We're stuck: efficient casing removal for well Abandonment applications. In: Offshore Technology Conference. Offshore Technology Conference.

Kaiser, M.J., 2015. Decommissioning forecast in the deepwater Gulf of Mexico, 2013–2033. Mar. Struct. 41, 96–126. https://doi.org/10.1016/j.marstruc.2014.12.006.

Kuanhai, D., Yue, Y., Yi, H., Zhonghui, L., Yuanhua, L., 2020. Experimental study on the integrity of casing-cement sheath in shale gas wells under pressure and temperature cycle loading. J. Petrol. Sci. Eng. 195, 107548. https://doi.org/10.1016/j.petrol.2020.107548.

Kunz, D., 2017. Well Abandonment Tool and Method of Use. WO 2017/091911 A1).

Kupresan, D., Heathman, J., Radonjic, M., 2014. Experimental assessment of casing expansion as a solution to microannular gas migration. In: IADC/SPE Drilling Conference and Exhibition, 4-6 March. Society of Petroleum Engineers, Fort Worth, Texas, USA. https://doi.org/10.2118/168056-MS.

Kupresan, D., Heathman, J., Radonjic, M., 2013. Application of a new physical model of expandable casing technology in mitigation of wellbore leaks. J. Can. Energy Technol. Innov. 1.

Ladva, H.K.J., Craster, B., Jones, T.G.J., Goldsmith, G., Scott, D., 2005. The cement-to-formation interface in zonal isolation. SPE Drill. Complet. 20 https://doi.org/10.2118/88016-PA.

Lecampion, B., Bunger, A., Kear, J., Quesada, D., 2013. Interface debonding driven by fluid injection in a cased and cemented wellbore: modeling and experiments. Int. J. Greenh. Gas Control 18, 208–223. https://doi.org/10.1016/j.ijggc.2013.07.012.

Li, Y., Lu, Y., Ahmed, R., Han, B., Jin, Y., 2019. Nonlinear stress-strain model for confined well cement. Materials (Basel). 12, 2626.

Ling, Y., 1996. Uniaxial true stress-strain after necking. AMP J. Technol. 5, 37–48.

Liversidge, D., Taoutaou, S., Agarwal, S., 2006. Permanent plug and abandonment solution for the north sea. In: SPE Asia Pacific Oil & Gas Conference and Exhibition, 11-13 September. Society of Petroleum Engineers, Adelaide, Australia. https://doi.org/10.2118/100771-MS.

Mathews, W.H., 1986. Physiography of the Canadian cordillera. Geological survey of Canada, map 1701A. Geol. Can. Cordilleran orogen Canada. In: Gabrielse, H., Yorath, C.J. (Eds.), Geol. Surv. Canada, Geol. Canada, vol. 4, pp. 403–418.

Montgomery, C.T., 2006. Implications of cementing for well production and performance. In: Nelson, E.B., Guillot, D. (Eds.), Well Cementing. Schlumberger, Sugar Land. TX 77478, USA, p. 773.

Natural Resources Canada, 2019. Technology Roadmap to Improve Wellbore Integrity: Summary Report. Energy.

Nelson, E.B., Guillot, D., 2006. In: Well Cementing, second ed. Schlumberger, Sugar Land, TX 77478, USA.

Nelson, J.F., Jørpeland, J.-T., Schwartze, C., 2018. Case history: a new approach to section milling: leaving the swarf behind!. In: Offshore Technology Conference. Offshore Technology Conference.
Obodozie, I.E., Trahan, S.J., Joppe, L.C., 2016. Eliminating sustained casing pressure in well abandonment. In: Offshore Technology Conference Asia. Offshore Technology Conference.
Orlic, B., 2009. Some geomechanical aspects of geological CO2 sequestration. KSCE J. Civ. Eng. 13, 225–232. https://doi.org/10.1007/s12205-009-0225-2.
Pardue, G.H., Morris, R.L., 1963. Cement bond log-a study of cement and casing variables. J. Petrol. Technol. 15, 545–555.
Procesi, M., Cantucci, B., Buttinelli, M., Armezzani, G., Quattrocchi, F., Boschi, E., 2013. Strategic use of the underground in an energy mix plan: synergies among CO2, CH4 geological storage and geothermal energy. Latium Region case study (Central Italy). Appl. Energy 110, 104–131. https://doi.org/10.1016/j.apenergy.2013.03.071.
Rairigh, J.G., 2020a. Shaped Charge Assembly, Explosive Units, and Methods for Selectively Expanding Wall of a Tubular (WO 2020/037267 A1).
Rairigh, J.G., 2020b. Duel End Firing Explosive Column Tools and Methods for Selectively Expanding a Wall of Tubular (WO 2020/037143 A1).
Ravi, K., Bosma, M., Gastebled, O., 2002. Safe and Economic Gas Wells through Cement Design for Life of the Well. SPE 75700.
Reddy, B.R., Xu, Y., Ravi, K., Gray, D.W., Pattillo, P., 2007. Cement Shrinkage measurement in oil well cementing-A comparative study of laboratory methods and procedures. In: Rocky Mountain Oil & Gas Technology Symposium. Society of Petroleum Engineers.
Roke Technologies, 2020. Vent Nanny V3 [WWW Document]. https://roke.ca/products-services/. accessed 5.6.2020.
Ruckert, F., 2020. Method for Remediating Leaks in a Cement Sheath Surrounding a Wellbore Tubular. WO 2020/016169 A1).
Ruggieri, C., 2004. Numerical investigation of constraint effects on ductile fracture in tensile specimens. J. Brazilian Soc. Mech. Sci. Eng. 26, 190–199.
Rushing, J.A., Newsham, K.E., Lasswell, P.M., Cox, J.C., Blasingame, T.A., 2004. Klinkenerg-corrected permeability measurements in tight gas sands: steady-state versus unsteady-state techniques. In: SPE Annual Technical Conference and Exhibition. Society of Petroleum Engineers.
Saponja, J., 1999. Surface casing vent flow and gas migration remedial elimination-new technique proves economic and highly successful. J. Can. Pet. Technol. 38.
Slater, H.J., 2010. The recommended practice for surface casing vent flow and gas migration intervention. In: SPE Annual Technical Conference and Exhibition. Society of Petroleum Engineers.
Smith, I., Olstad, E., Segura, R., 2011. Heightened regulations create demand for well abandonment services. In: Offshore(Tulsa), vol. 71.
Song, H.-W., Kim, J.-H.J., Choi, J.-H., Byun, K.-J., 2001. Microscopic analysis of 50% axially strained cementitious materials. Cement Concr. Res. 31, 1191–1202.
Taylor, H.F.W., 1992. Cement Chemistry. Academic Press Limited, London, UK.
Toor, I.A., 1983. Problems in squeeze cementing. In: Middle East Oil Technical Conference and Exhibition. Society of Petroleum Engineers.
Torsæter, M., Todorovic, J., Lavrov, A., 2015. Structure and debonding at cement–steel and cement–rock interfaces: effect of geometry and materials. Construct. Build. Mater. 96, 164–171.
van Eijden, J., Cornelissen, E., Ruckert, F., Wolterbeek, T., 2017. Development of experimental equipment and procedures to evaluate zonal isolation and well Abandonment materials. In: SPE/IADC Drilling Conference and Exhibition. Society of Petroleum Engineers, pp. 14–16. https://doi.org/10.2118/184640-MS.
Vrålstad, T., Saasen, A., Fjær, E., Øia, T., Ytrehus, J.D., Khalifeh, M., 2019. Plug & abandonment of offshore wells: ensuring long-term well integrity and cost-efficiency. J. Petrol. Sci. Eng. 173, 478–491.
Wang, W., Taleghani, A.D., 2014. Three-dimensional analysis of cement sheath integrity around Wellbores. J. Petrol. Sci. Eng. 121, 38–51.
Warne, P., 2004. Decommissioning - north sea. Oil, Gas Energy Law J. 2.
Winarga, K., Dewanto, C.W., 2010. Surfactant treatment has amazingly improved squeeze cementing result. In: Nigeria Annual International Conference and Exhibition. Society of Petroleum Engineers.
Wise, J., Cedola, A., Nygaard, R., Hareland, G., Arild, Ø., Lohne, H.P., Ford, E.P., 2020. Wellbore characteristics that control debonding initiation and microannuli width in finite element simulations. J. Petrol. Sci. Eng. 191, 107157. https://doi.org/10.1016/j.petrol.2020.107157.
Wojtanowicz, A.K., Nishikawa, S., Rong, X., 2001. Diagnosis and Remediation of Sustained Casing Pressure in Wells. Final Report. Louisiana State Univ. Virginia. Submitt. to US Dep. Inter. Miner. Manag. Serv.. https://www.bsee.gov/sites/bsee.gov/files/tap-technical-assessment-program/008dk.pdf
Wolterbeek, T.K.T., Hangx, S.J.T., Spiers, C.J., 2016. Effect of CO2-induced reactions on the mechanical behaviour of fractured wellbore cement. Geomech. Energy Environ. 7, 26–46. https://doi.org/10.1016/j.gete.2016.02.002.
Wolterbeek, T.K.T., Raoof, A., 2018. Meter-scale reactive transport modeling of CO2-rich fluid flow along debonded wellbore casing-cement interfaces. Environ. Sci. Technol. 52, 3786–3795. https://doi.org/10.1021/acs.est.7b05358.
Wolterbeek, T.K.T., Ruckert, F., van Moorsel, S.G., Cornelissen, E.K., 2019. Reactive transport and permeability evolution in wellbore defects exposed to periodic pulses of CO2-rich water. Int. J. Greenh. Gas Control 91, 102835. https://doi.org/10.1016/j.ijggc.2019.102835.
Wolterbeek, T.K.T., van Noort, R., Spiers, C.J., 2018. Reaction-driven casing expansion: potential for wellbore leakage mitigation. Acta Geotech. 1–26. https://doi.org/10.1007/s11440-017-0533-5.
Zeng, Y., Liu, R., Li, X., Zhou, S., Tao, Q., Lu, P., 2019. Cement sheath sealing integrity evaluation under cyclic loading using large-scale sealing evaluation equipment for complex subsurface settings. J. Petrol. Sci. Eng. 176, 811–820. https://doi.org/10.1016/j.petrol.2019.02.014.
Zhang, M., Bachu, S., 2011. Review of integrity of existing wells in relation to CO2 geological storage: what do we know? Int. J. Greenh. Gas Control 5, 826–840. https://doi.org/10.1016/j.ijggc.2010.11.006.